

1 **Insights into characteristics and formation mechanisms of secondary organic**
2 **aerosols in Guangzhou urban area**

3 **Miaomiao Zhai^{1,3}, Ye Kuang^{1,3*}, Li Liu^{2,*}, Yao He^{1,3}, Biao Luo^{1,3}, Wanyun Xu⁴, Jiangchuan**
4 **Tao^{1,3}, Yu Zou², Fei Li^{2,5}, Changqin Yin^{2,7}, Chunhui Li², Hanbing Xu⁶, Xuejiao Deng²**

5 ¹ Institute for Environmental and Climate Research, Jinan University, Guangzhou, China.

6 ² Key Laboratory of Regional Numerical Weather Prediction, Institute of Tropical and Marine
7 Meteorology, China Meteorological Administration, Guangzhou, 510640, China

8 ³ Guangdong-Hongkong-Macau Joint Laboratory of Collaborative Innovation for Environmental
9 Quality, Guangzhou, China.

10 ⁴ State Key Laboratory of Severe Weather & Key Laboratory for Atmospheric Chemistry, Institute of
11 Atmospheric Composition, Chinese Academy of Meteorological Sciences, Beijing, 100081, China

12 ⁵ Xiamen Key Laboratory of Straits Meteorology, Xiamen Meteorological Bureau, Xiamen, 361012,
13 China

14 ⁶ Experimental Teaching Center, Sun Yat-Sen University, Guangzhou 510275, China

15 ⁷ Shanghai Key Laboratory of Meteorology and Health, Shanghai Meteorological Bureau, Shanghai
16 200030, China

17 *Correspondence to: Ye Kuang (kuangye@jnu.edu.cn) and Li Liu (liul@gd121.cn)

18
19
20
21
22
23
24
25
26
27
28
29
30
31
32
33
34
35
36
37

38 **Abstract**

39 Emission controls have substantially brought down aerosol pollution in China, however, aerosol
40 mass reductions have slowed down in recent years in the Pearl River Delta (PRD) region, where
41 secondary organic aerosol (SOA) formation poses a major challenge for air quality improvement. In
42 this study, we characterized the roles of SOA in haze formation in urban Guangzhou City of the PRD
43 using year-long aerosol mass spectrometer measurements for the first time and discussed possible
44 pathways of SOA formations. On average, organic aerosols (OA) contribute dominantly (50%) to non-
45 refractory submicron aerosol mass (NR-PM₁). The average mass concentration of SOA (including by
46 less and more oxidized OA, LOOA and MOOA) contributed most to NR-PM₁, ~~reaching~~reached about
47 1.7 times that of primary organic aerosols (POA, including hydrocarbon-like and cooking-related OA)
48 and accounting for 32% of NR-PM₁, even more than sulfate (22%) and nitrate (16%). Seasonal
49 variations of NR-PM₁ revealed that haze formation mechanisms differed much among distinct seasons.
50 Sulfate mattered more than nitrate in fall, while nitrate was more important than sulfate in spring and
51 winter, with SOA contributing significantly to haze formations in all seasons. Daytime SOA formation
52 was weak in winter under low oxidant level and air relative humidity, whereas prominent daytime SOA
53 formation was observed in fall, spring and summer almost on daily basis, suggesting for important
54 roles of photochemistry in SOA formations. Further analysis showed that the coordination of gas-phase
55 photochemistry and subsequent aqueous-phase reactions likely played significant roles in quick
56 daytime SOA formations. Obvious nighttime SOA formations were also frequently observed in spring,
57 fall and winter, and it was found that daytime and nighttime SOA formations together had resulted in
58 the highest SOA concentrations in these seasons and contributed substantially to severe haze
59 formations. Simultaneous increases of nitrate with SOA after sunset suggested the important roles of
60 NO₃ radical chemistry in nighttime SOA formations, and confirmed by continuous increase of
61 NO⁺/NO₂⁺ fragment ratio that related to measured particulate nitrate after sunset. Findings of this study
62 have promoted our understanding in haze pollution characteristics of the PRD and laid down future
63 directions on investigations of SOA formation mechanisms in urban areas of southern China that share
64 similar emission sources and meteorological conditions.

65

66 **1 Introduction**

67 Ubiquitous submicron aerosols in the atmosphere not only deteriorate human health and visibility,
68 but also impact climate through interactions with solar radiation and clouds. Organic aerosols (OA)
69 represent one of the most important and sometimes even dominant components (~10-90%) of PM₁
70 (aerosol particles with aerodynamic diameter less than 1 μm) in urban, rural and remote areas (Zhang
71 et al., 2007; Jimenez et al., 2009). OA can either be emitted directly from emission sources or be formed
72 through atmospheric reactions of volatile organic compounds, the former is referred to as primary OA
73 (POA) and the latter is referred to as secondary OA (SOA). An increasing number of researches show
74 that SOA account for a large fraction of OA worldwide (Zhang et al., 2007; Zhang et al., 2011), and
75 even dominate in some cases (Kuang et al., 2020). The implementation of strict emission reduction
76 policies has significantly improved the air quality of Pearl River Delta (PRD) region, which is a highly
77 industrialized area of China, and the annual mean concentration of PM_{2.5} (particulate matter with
78 aerodynamic diameter less than 2.5 μm) has been brought down to less than 30 μg/m³ (Xu et al., 2020).
79 However, the reduction of PM_{2.5} mass concentrations in PRD has slowed down substantially in recent
80 years, which might be related to the significant increases in the proportion of secondary aerosols (Xu
81 et al., 2020), especially for SOA. ~~However, long-term observations that elucidate the sources and~~
82 ~~secondary formations of OA in this area is still missing~~ Insights into SOA formation mechanisms are
83 important for air pollution improvement.

84 SOA formation mechanisms are a scientific hotspot of atmospheric chemistry in recent ten years
85 since significant contributions of SOA to atmospheric aerosol mass were fully recognized (Zhang et
86 al., 2007; Jimenez et al., 2009), however quite complex due to varying precursors, oxidants and
87 formation pathways under different emission characteristics and meteorological conditions. As to SOA
88 formation pathways, SOA can be formed through condensation of oxidized gas-phase organic vapors
89 during the oxidation of volatile organic compounds (VOCs), this type of formed SOA was usually
90 referred to as gasSOA (Kuang et al., 2020). SOA can also be formed in the aqueous phase through the
91 further oxidation of dissolved VOCs which are usually products of gas-phase oxidation of VOCs, this
92 type of SOA was usually referred as aqSOA (Ervens et al., 2011). Both field measurements and
93 laboratory studies are needed in investigating detailed SOA formation mechanisms in different regions
94 with field measurements provide insights into key oxidants and formation pathways, thus information

95 from field measurements are important for both designing laboratory experiments and targeting
96 emission control strategies. Aerosol mass spectrometers are advanced on-line instruments that provide
97 real time quantitative characterization of aerosol particle compositions (Jayne et al., 2000;Canagaratna
98 et al., 2007;Jimenez et al., 2003). Positive matrix factorization (PMF) (Ulbrich et al., 2009) or a
99 multilinear engine (ME-2) (Paatero, 1999;Canonaco et al., 2013) can be employed to further resolve
100 different OA factors that are associated with different sources and formation mechanisms from the OA
101 mass spectra. ~~Although aerosol mass spectrometers have been widely used in China in recent years,~~
102 ~~most studies have been conducted in specific periods due to its high cost and maintenance (He et al.,~~
103 ~~2011;Chen et al., 2021;Qin et al., 2017), resulting in few long-term characterizations of the mass~~
104 ~~concentrations and chemical compositions of PM_{2.5}. The design of Aerosol Chemical Speciation~~
105 ~~Monitor (ACSM) has improved this problem to some extent (Ng et al., 2011;Sun et al., 2015). Based~~
106 ~~on 2-year ACSM measurements, Using this technique, the SOA sources and formation mechanisms~~
107 ~~are extensively investigated in China (Zhou et al., 2020), and found that aqueous reactions in aerosol~~
108 ~~water contributed substantially even dominantly to SOA formations (Su et al., 2020) in haze episodes~~
109 ~~with daytime and nighttime SOA formations differ much due to different meteorological conditions~~
110 ~~and oxidants Sun(Rollins et al.(2018., 2012;Huang et al., 2021) investigate the distinct characteristics~~
111 ~~of PM_{2.5} compositions among different seasons in Beijing urban area. Canonaco et al. (2021) also~~
112 ~~performed a long-term source apportionment on a 1-year ACSM dataset from downtown Zurich. Many~~
113 ~~other studies also have successfully applied the ACSM in the monitoring organic aerosols in various~~
114 ~~regions (Sun et al., 2012;Sun et al., 2013;Sun et al., 2014;Sun et al., 2016;Fröhlich et al., 2013;Allan~~
115 ~~et al., 2010;Zhang et al., 2012;Xu et al., 2015a;Zhou et al., 2020;Huang et al., 2014;Hu et al., 2016;Via~~
116 ~~et al., 2021), however long-term measurements are still relatively scarce, and remain missing in urban~~
117 ~~areas of the PRD region.~~

118 Guo et al. (2020) found that OA played a dominant role in PM_{2.5} during winter in Guangzhou, a
119 mega-city of the PRD, and the results of OA source apportionment emphasized the dominance of SOA.
120 Qin et al. (2017) and Huang et al. (2011) also reported similar results during autumn and winter in
121 Guangzhou. In fact, in a specific region, the compositions, sources, and evolution processes
122 differ much among seasons due to changes in emission sources and meteorological conditions (Li et
123 al., 2015). ThusTherefore, long-term characterizations-observations that cover measurements of

带格式的：缩进：首行缩进： 2 字符

124 different seasons ~~are urgently~~ were usually needed ~~to gain insights into emission~~ for characterizing OA
125 sources and SOA formation mechanisms ~~of OA~~, thereby helping to address the challenge of fine
126 particulate matter pollution mitigation. ~~Even though aerosol mass spectrometers have been widely~~
127 ~~used in China in recent years and the PRD region,~~ importance of long-term measurements, most studies
128 ~~have been conducted in specific periods due to its high cost and maintenance (He et al., 2011; Chen et~~
129 ~~al., 2021b; Qin et al., 2017), resulting in few long-term characterizations of the mass concentrations~~
130 ~~and chemical compositions of submicron particulate matter (PM₁). The design of Aerosol Chemical~~
131 ~~Speciation Monitor (ACSM) has improved this problem to some extent (Ng et al., 2011; Sun et al.,~~
132 ~~2015; Canonaco et al., 2021). For example, based on 2-year ACSM measurements, Sun et al. (2018)~~
133 ~~investigate the distinct characteristics of PM₁ compositions among different seasons in Beijing urban~~
134 ~~area and illustrated the dominant role of SOA in OA across different mass loading scenarios during all~~
135 ~~seasons.~~

136 Guangzhou is an expansive metropolis in the highly industrialized PRD region. Using the aerosol
137 mass spectrometer measurements and source apportionment technique, Qin et al. (2017) and Huang et
138 al. (2011) reported that SOA contributed substantially to aerosol mass during autumn and winter in
139 Guangzhou. Guo et al. (2020) found that OA played a dominant role in PM₁ during winter in
140 Guangzhou, with OA source apportionment emphasized the dominance of SOA. Guo et al. (2020) also
141 suggested that gasSOA contributed predominantly to SOA formation during non-pollution periods,
142 other mechanisms such as heterogeneous and multiphase reactions played more important roles in
143 SOA formation during pollution episodes, however long-term aerosol spectrometer measurements hat
144 help for characterizing OA source and SOA formation mechanisms in this region remain lacking. In
145 this study, we performed a year-long continuous measurement of non-refractory submicron aerosols
146 (NR-PM₁) with an ACSM in urban Guangzhou from September 2020 to August 2021 to characterize
147 POA sources and investigate SOA formation mechanisms in different seasons.

148 2 Experimental methods

149 2.1 sampling site and measurements

150 A quadrupole-Aerosol Chemical Speciation Monitor (Q-ACSM) was deployed to continuously

151 measure nonrefractory PM₁ (NR-PM₁) species including OA, sulfate (SO₄), nitrate (NO₃), ammonium
152 (NH₄), and chloride (Cl) from September 2020 to August 2021 at an urban site located in Haizhu
153 wetland park of Guangzhou, which is surrounded by commercial streets and residential buildings,
154 however, with a distance of at least 1 km (Liu et al., 2022). Therefore, measurements at this site are
155 representative of the pollution characteristics of Guangzhou urban area. More detailed descriptions
156 about the sampling site and the ACSM measurements could be referred to Liu et al. (2022) and Ng et
157 al. (2011), respectively. An AE33 aethalometer (Drinovec et al., 2015) set up with a flow rate of 5
158 L/min was separately operated downstream of a PM_{2.5} inlet (BGI SCC 1.829) to measure aerosol
159 absorptions, from which optically equivalent black carbon (BC) mass concentrations in winter and
160 early spring were calculated. In addition, mass concentrations of PM_{2.5} and trace gases such as nitrogen
161 dioxide (NO₂), ozone (O₃), carbon monoxide (CO) and sulfur dioxide (SO₂) were acquired from the
162 publicly available datasets of the China National Environmental Monitoring network
163 (<http://www.cnemc.cn/en/>), which includes a site located within 5 km distance to our observation site.
164 Measurements of meteorological parameters such as temperature, wind speed and direction (WS and
165 WD), and relative humidity (RH) were made by an automatic weather station (Li et al., 2021). Aerosol
166 liquid water content (ALWC) was predicted with the ISORROPIA-II thermodynamic model in reverse
167 mode under metastable assumption (Guo et al., 2017) with aerosol chemical compositions measured
168 by Q-ACSM as inputs, with more details in Supplement Sect.S2.

169 **2.2 Q-ACSM data analysis**

170 The Q-ACSM data were processed using ACSM standard data analysis software (ACSM Local
171 1.5.10.0 Released July 6, 2015) written in Igor Pro (version 6.37). The composition-dependent
172 collection efficiency (CE) parameterization scheme proposed by Middlebrook et al. (2012) was chosen
173 to determine the mass concentrations of NR-PM₁ species which was also detailed in Liu et al. (2022).
174 Relative ionization efficiencies (RIEs) of 5.15 and 0.7 were adopted for ammonium and sulfate
175 quantifications which were calibrated using 300 nm pure NH₄NO₃ and (NH₄)₂SO₄ while the default
176 RIEs of 1.4, 1.1 and 1.3 was used for organic aerosol, nitrate and chloride, respectively. Moreover, we
177 also compared the mass concentrations of NR-PM₁ with PM_{2.5} to ensure the validity of ACSM data
178 during the whole study. As shown in Fig. S1 of the supplement, the measured NR-PM₁ correlates

179 highly with $PM_{2.5}$ acquired from the nearest (about 5 km) Environmental Protection Agency site ($R^2 =$
 180 0.71), and the average ratio of $NR-PM_1/PM_{2.5}$ is $0.77 (\pm 0.36)$.

181 Unconstrained Positive matrix factorization (PMF) was performed on OA mass spectra of the
 182 entire year-long dataset. For the two-factor solution, the POA factor peaked in the evening with low
 183 O/C (~ 0.28) and an oxygenated OA (OOA) factor peaks in the afternoon with high O/C (~ 0.88) can
 184 be well resolved (Fig.S2), demonstrating the markedly different influences of primary emissions and
 185 SOA formations on diel aerosol mass concentrations. However, PMF-ACSM analysis of mass spectra

带格式的: 缩进: 首行缩进: 2 字符

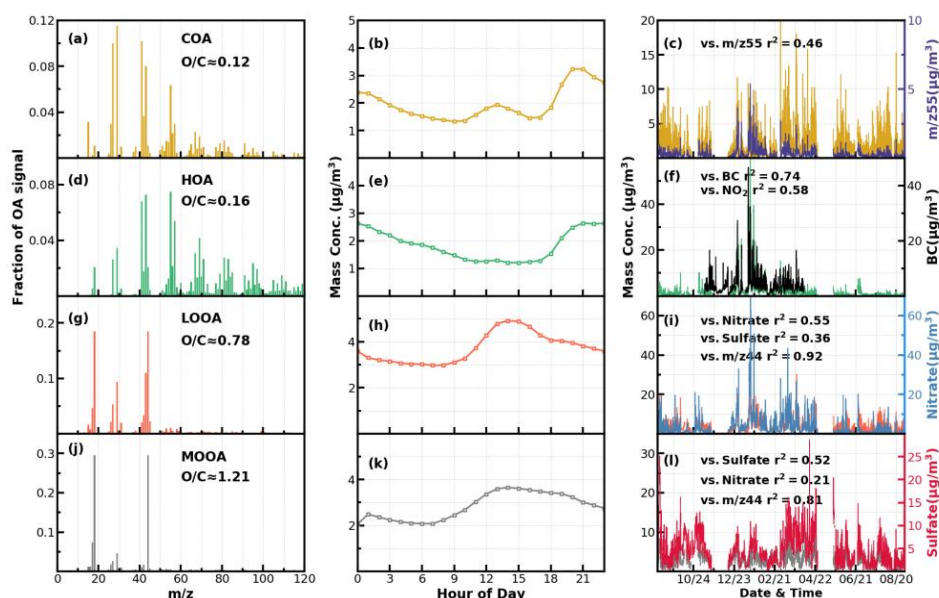


Figure 1. Mass spectral profiles, diurnal cycles and correlations with external data of COA (a-c), HOA (d-f), LOOA (g-i) and MOOA (j-l) from ME2-ACSM analysis for the entire year.

186 of OA measured by unit mass resolution instruments still faced some uncertainties to further resolve
 187 potential POA or SOA components due to its rotational indeterminacy. For example, traffic-related
 188 hydrocarbon-like organic aerosols (HOA) was uneasily to separate from cooking-related organic
 189 aerosols (COA) and there was also great uncertainty in distinguishing SOA with different degrees of
 190 oxidations (Sun et al., 2012; Sun et al., 2013; Zhang et al., 2015). Therefore, an improved source
 191 apportionment technique called Multilinear Engine (ME-2) was further used to resolve better sources
 192 of POA and SOA (Paatero, 1999; Canonaco et al., 2013; Guo et al., 2020). Previously, both Guo et al.

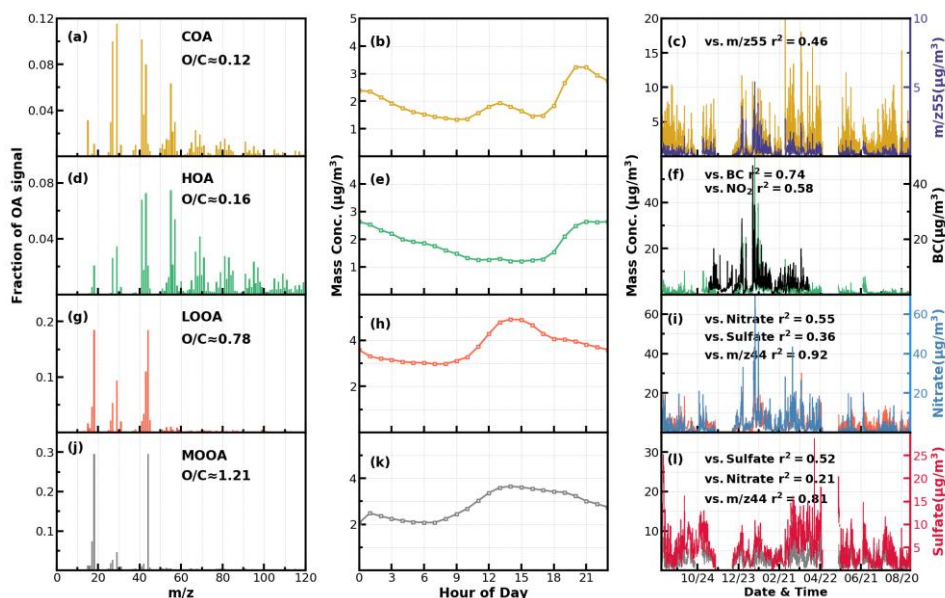


Figure 1. Mass spectral profiles, diurnal cycles and correlations with external data of COA(a-c), HOA(d-f), LOOA(g-i) and MOOA(j-l) from ME2-ACSM analysis for the entire year.

193 (2020) and Liu et al. (2022) demonstrated that during both autumn and winter seasons of Guangzhou
 194 urban areas, POA was mainly composed of HOA, which is mostly associated with traffic emissions
 195 and COA, and SOA could be resolved into less oxidized and more oxidized organic aerosols (LOOA
 196 and MOOA). The number selecting test using unconstrained PMF analysis (Fig.S3) also showed that
 197 four-factor solution likely be the best choice. Therefore, we had chosen 4 factors for ME-2 analysis
 198 with the α value of ME-2 ranges from 0.1 to 0.5, and constrained the HOA and COA profiles with
 199 HOA and COA profiles reported in Liu et al. (2022) as priories considering the following three reasons:
 200 (1) The used instrument of this study is the same one of Liu et al. (2022); (2) the COA profile reported
 201 in Liu et al. (2022) was determined during the period when both COVID-19 silence-action and festival
 202 spring occurred when cooking activities grew and traffic activities almost vanished thus COA shall
 203 dominated over HOA, more details about the method please refer to Liu et al. (2022); (3) Resolved
 204 variations of HOA and COA are well explained by external datasets such as correlations of HOA with
 205 black carbon reached 0.79. The four-factor solution using the ME-2 technique with $\alpha=0.2$ was obtained
 206 and shown in Fig.1. The resolved HOA and COA are summed as POA, resolved LOOA and MOOA

207 are summed as SOA, and the comparison with those resolved by the PMF is shown in Fig.2. ME-2
 208 analysis generally reproduced both the diurnal variations as well as absolute mass concentrations of
 209 POA and SOA during different months well. To explore the consistency of resolved factors using the
 210 entire year-long dataset or only using seasonal dataset when performing ME-2 analysis, we performed
 211 individual ME-2 runs for each season. Results showed that factors resolved in each season using
 212 seasonal datasets as inputs of ME-2 are generally consistent with those resolved from year-long dataset
 213 (Fig.S4-S7). Therefore, factors resolved using the entire year-long dataset as input of ME-2 were used
 214 for further investigations and this also guaranteed consistency of factors for comparisons among
 215 seasons.

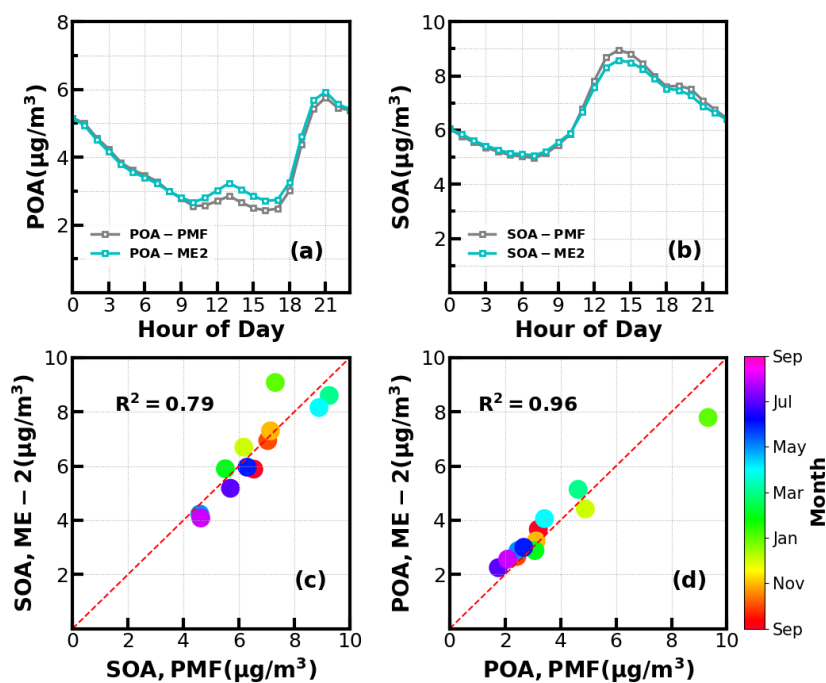


Figure 2. (a) and (b) Diurnal variations of POA and SOA concentrations from ME-2 and PMF; (c) and (d) Scatter plots between monthly average POA and SOA concentrations from ME-2 and PMF.

216 The mass spectrum of COA deconvolved in this work was characterized by a high m/z 55-to-57
 217 ratio of 2.12, which was the same with the one reported by Guo et al. (2020), and close to the m/z 55-
 218 to-57 ratio range of 2.2-2.8 reported by Mohr et al. (2012) for COA. Similar to previous studies (Guo
 219 et al., 2020; Sun et al., 2013), the concentration of COA was well correlated ($R^2=0.46$) with m/z 55.

220 The O/C ratio of 0.12 for COA revealed that it was less oxidized than HOA (O/C=0.16) during the
 221 whole year in Guangzhou, which was contrary to Sun et al. (2011). As shown in Fig.3, the diurnal
 222 profile of COA presented two typical peaks during the entire year with a noontime peak during 13:00
 223 - 14:00 LT and an evening peak during 20:00 - 21:00 LT, which were associated with noon and evening
 224 cooking activities. It was noteworthy that the nighttime peak concentration of COA was very close to
 225 that of noontime in summer, while the evening peak of COA was significantly higher than that of

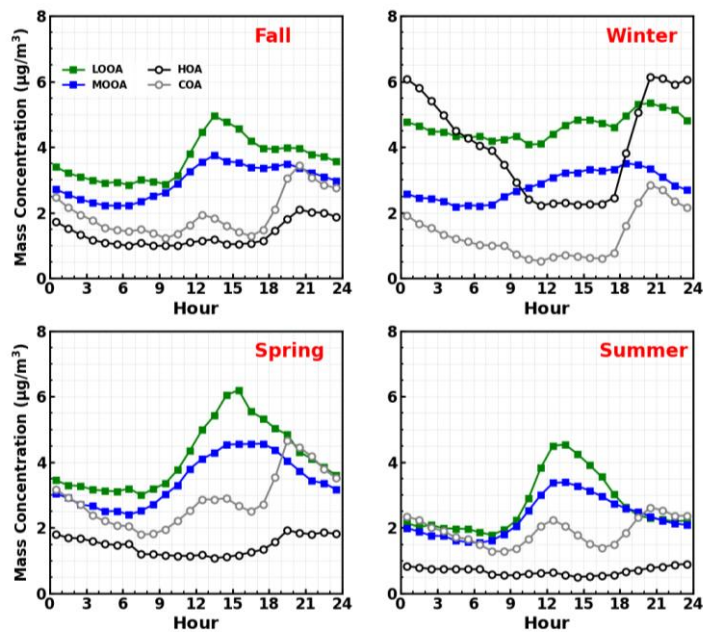


Figure 3. Diurnal profiles of HOA, COA, LOOA and MOOA in spring (March to May), summer (June to August), Fall (September to November), Winter (December to February).-

226 noontime in other three seasons. The ratio of evening COA peak to that of the noontime was 1.7 in fall,
 227 and was 1.6 in spring. In particular, the evening COA peak was nearly 4 times that of noontime in
 228 winter due to the relatively insignificant noontime peak during this period, which might be associated
 229 with the lock down and spring festival in winter which resulted in less noontime activities. Similar
 230 conclusions could be found in Sun et al. (2018). More frequent cooking activities at night such as the
 231 Chinese habit of eating midnight snacks, shallower boundary layer that inhibited diffusion of pollutants,
 232 and the lower temperature at night which facilitated semi-volatile compounds from cooking emissions
 233 to partition into particles resulted in the higher peak concentration at nighttime than at noon (Guo et

234 al., 2020).

235 The mass spectrum of HOA (Fig.1b) was characterized with the $C_nH_{2n-1}^+$ ($m/z = 27, 41, 55, 69$)
236 and $C_nH_{2n+1}^+$ ($m/z = 29, 43, 57, 71$) ion species. The concentration of HOA had a good correlation
237 with that of primary BC emission ($R^2=0.74$), and also correlated well with that of NO_2 ($R^2=0.58$),
238 indicating considerable impacts of traffic emissions on the HOA mass loading. As shown in Fig.3,
239 except for summer, HOA increased significantly after sunrise especially in winter, however, began to
240 decrease in the late evening. HOA was significantly higher during nighttime than during daytime in
241 all seasons especially in winter, however, was not obvious in summer. HOA mass concentration peaks
242 around 20:00 LT were attributed to traffic emissions during the nocturnal rush hours. However, the
243 continuously high concentrations of HOA after 20:00 until 02:00 of the next day might have resulted
244 from heavy-duty vehicles with daytime traffic restrictions in Guangzhou (Guo et al., 2020;Qin et al.,
245 2017).

246 Two OOA factors were characterized with high O/C ratio, LOOA with O/C of 0.78 and MOOA
247 with O/C of 1.2, suggesting high oxidation degrees of SOA factors in Guangzhou urban area, especially
248 that of MOOA. MOOA and LOOA shared similar diurnal profiles regardless of seasons, with MOOA
249 showed higher correlations with sulfate and LOOA showed higher correlations with nitrate. MOOA
250 and LOOA increased together in fall from 09:00 LT until 14:00 LT reached a maximum of $3.7 \mu\text{g}/\text{m}^3$
251 for MOOA and $5 \mu\text{g}/\text{m}^3$ for LOOA, followed by a gradual decrease in SOA concentrations and then
252 remained relatively flat. The diurnal profiles of SOA in spring and summer were relatively similar to
253 those in fall, however, more remarkable decreases of SOA from afternoon to midnight were observed
254 in spring and summer. This is because SOA sometimes increased after sunset in autumn, which was
255 even more prominent in winter, where LOOA and MOOA would first increase for a while after sunset
256 and then begun to decrease. However, weaker daytime SOA formation was observed in winter. -Note
257 that a aqSOA factor (called aqOOA in these references) was previously resolved using the aerosol
258 mass spectrometer measurements (Sun et al., 2016;Zhao et al., 2019) or time-of flight ACSM
259 measurements (Lei et al., 2021), and the factor was resolved as aqSOA because of its high fraction of
260 m/z 29 (CHO+) and high correlation with sulfate. Both two resolved SOA factors in this study showed
261 relatively weak correlations with sulfate (Fig.1), do not support directly if they are related with aqueous
262 phase reactions.

263 3 Results and discussion

264 3.1 The largest contribution of secondary organic aerosols in NR-PM₁

265 Time series of the meteorological parameters (including RH, WS and WD), the mass
266 concentrations of NR-PM₁ and PM_{2.5}, chemical compositions of NR-PM₁, trace gases and four
267 resolved OA factors are shown Fig.S8. It shows that emission source intensities and meteorological
268 variables changed dramatically among seasons. Hourly NR-PM₁ mass concentrations ranged from near
269 zero to 177 $\mu\text{g}/\text{m}^3$ with an average of 21 $\mu\text{g}/\text{m}^3$. From October to February, northerly winds prevailed
270 and average NR-PM₁ was relatively higher than that from February to September (26 vs 19 $\mu\text{g}/\text{m}^3$),
271 which were associated with relatively lower boundary height during cold seasons and northern winds
272 brought polluted continental air mass. While during warm seasons of Guangzhou (March to
273 September), south-easterly wind prevailed, which brought cleaner air mass from the ocean and the
274 boundary layer height was higher due to more surface heating. Monthly variations of PM_{2.5} are shown
275 in Fig.3a4a, PM_{2.5} in summer was lowest and around 16 $\mu\text{g}/\text{m}^3$ from May to August which were likely
276 associated with the prevalence of rainy conditions in summer ~~and possible higher boundary layer~~
277 ~~height.(Fig.S9) and possible higher boundary layer height (Yang et al., 2013).~~ January was the month
278 with highest PM_{2.5} mass concentrations with an average of 49 $\mu\text{g}/\text{m}^3$, which was consistent with the
279 fact that winter usually experienced the worst air pollutions due to the stagnant air conditions.

The average mass contributions of different components to NR-PM₁ during the entire year and

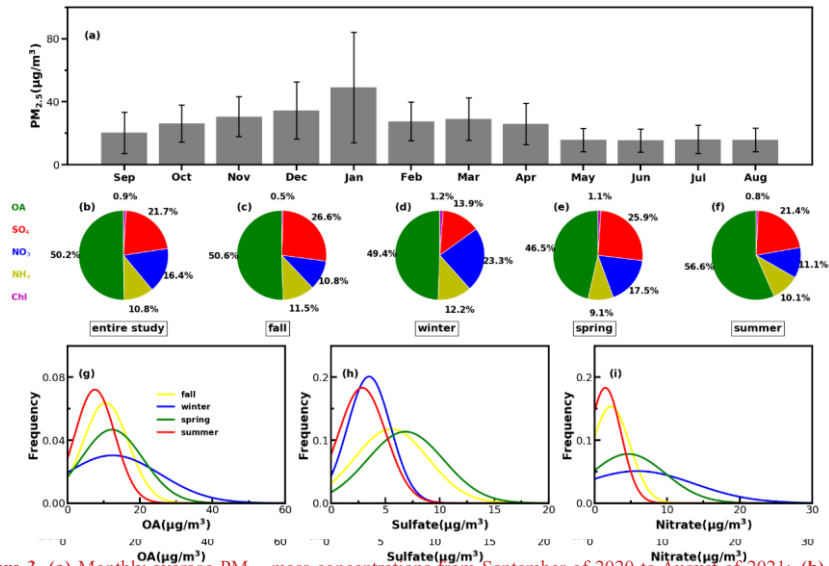


Figure 3. (a) Monthly average PM_{2.5} mass concentrations from September of 2020 to August of 2021; (b)–(f) The monthly mass contributions of the PM₁ chemical components (NR-PM₁) in the entire year and different seasons; (g)–(i) Average mass contributions of OA, sulfate (SO₄) and nitrate (NO₃) in different seasons; (g)–(i) Probability distributions of OA, sulfate (SO₄) and nitrate (NO₃) in different seasons.

among different seasons are shown in Fig. 3b–3f. On average OA contributed about 50% to NR-PM₁ with the highest contribution in summer that reached near 57% and lowest contribution in spring of about 47%. The second largest contributor was sulfate, which on average contributed about 22%, and more than 20% in spring, summer and fall. However, the contribution of nitrate to NR-PM₁ (23%) exceeded that of sulfate (14%) and became the second major component after OA in winter, consistent with the results of Guo et al. (2020) for pollution periods in winter of Guangzhou. The probability distributions of mass concentrations of OA, sulfate and nitrate are shown in Fig. 3g–3i. Both OA and nitrate were distributed in wide ranges during winter and shared similar shape of probability distribution, with OA increasing gradually from summer to winter and then reducing in the spring. Sulfate shared similar magnitudes in summer and winter, and differed much from those in spring and fall that had higher sulfate concentrations and varied in a wider range. Nitrate in summer and fall were relatively lower in summer and fall, however, had much higher concentrations in spring and winter.

293 As shown in Fig.4a5a, average OA concentrations of different months ranged from about 7 $\mu\text{g}/\text{m}^3$
 294 to 17 $\mu\text{g}/\text{m}^3$ with the peak in January and the lowest in August, and the variations of OA mass
 295 concentration in winter and spring were much larger than those in summer and autumn. Monthly

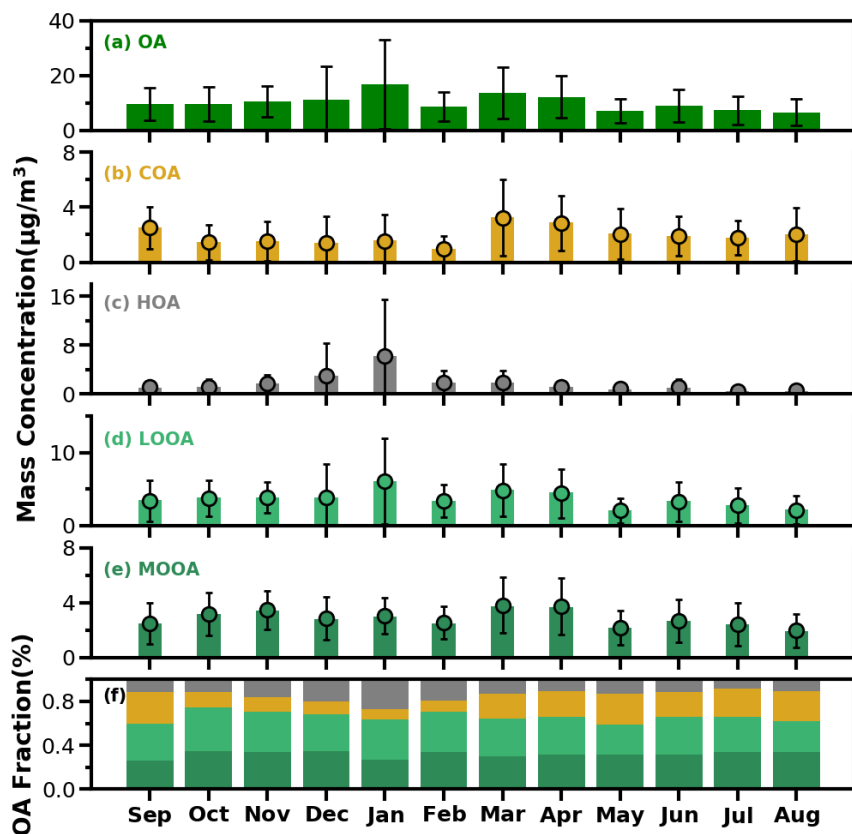


Figure 4. The bar plots of monthly average mass concentrations of OA, COA, HOA, LOOA and MOOA from (a) to (e) and mass fractions of OA factors in OA (f).—

296 variations of mass concentrations of the four resolved factors are shown in Fig.4b-e5b-5e, and
 297 contributions of the four OA factors to OA are shown in Fig.4f5f. In general, HOA remained lower
 298 than 2 $\mu\text{g}/\text{m}^3$ in most months, however, as the cold season approached from November, the monthly
 299 average OA increased substantially from about 2 $\mu\text{g}/\text{m}^3$ to near 6 $\mu\text{g}/\text{m}^3$. The much lower temperature
 300 and accumulation favorable meteorological conditions likely had resulted in the substantial increase
 301 of HOA. The obviously higher concentrations of NO_2 even under lower wintertime O_3 concentrations

302 ~~(Fig.S8) implied that more traffic emissions in winter might also had contributed to the substantial~~
303 ~~HOA increase.~~ Compared with HOA, the seasonal variations of COA were less pronounced. The
304 monthly average concentration of COA in warm months (February to October) was higher than those
305 in cold months (October to January). The lowest monthly average concentration of COA was about
306 $1 \mu\text{g}/\text{m}^3$ which occurred in February when the contribution of COA to OA was near its lowest of about
307 9%. Overall, COA contributed about 19% of OA during the whole year which was close to that of
308 HOA (18%). However, the contributions of COA and HOA to total OA differ much among seasons.
309 The contributions of COA to OA were higher than that of HOA during warm months, ~~however, and~~
310 lower than that of HOA in relatively cold months especially in winter, ~~and contributed about 19% of~~
311 ~~OA during the whole year, which was close to that of HOA (18%).~~ These results highlight the

312 significant contributions of POA to OA in Guangzhou urban area, however, contributions of emission
 313 sources differed much among cold and warm seasons.

314 SOA (MOOA+LOOA) contributed more than 60% to OA in all months, reached beyond 70% in
 315 October and February, and made up on average 63% of OA in the entire year. As shown in Fig.45(e-
 316 f), LOOA exhibited stronger seasonal variations than MOOA, with monthly average mass

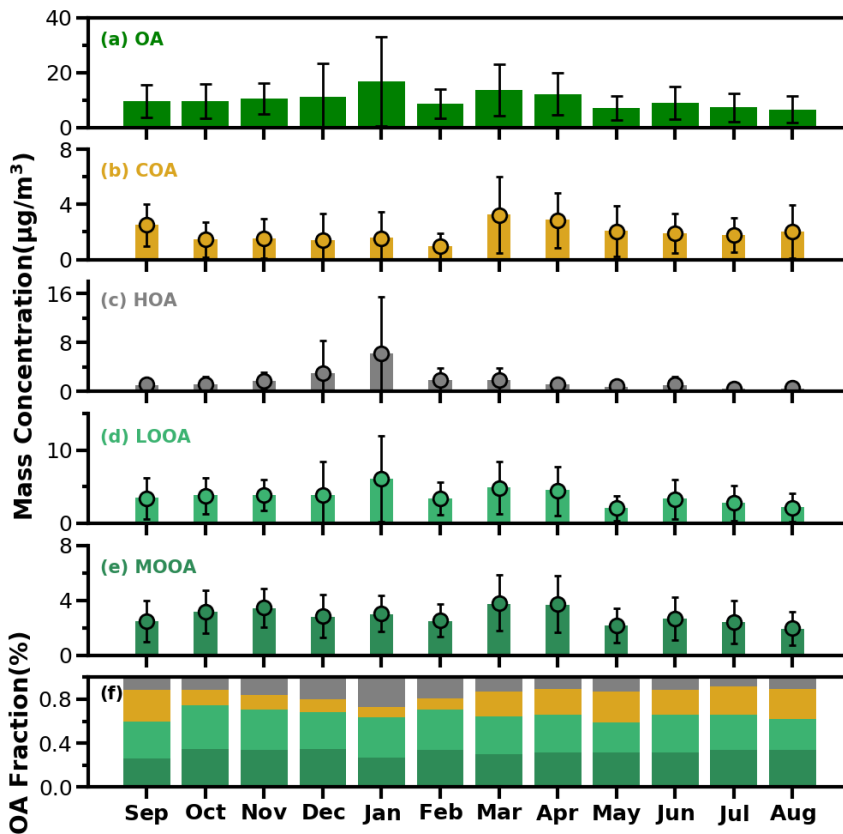


Figure 5. The bar plots of monthly average mass concentrations of OA, COA, HOA, LOOA and MOOA from (a) to (e) and mass fractions of OA factors in OA (f).

317 concentrations of LOOA varying between 2.6 to 6.1 $\mu\text{g}/\text{m}^3$ and monthly average MOOA concentration
 318 ranging from 2 to 3.8 $\mu\text{g}/\text{m}^3$. The LOOA mass concentration peaked in the most polluted month of
 319 January, suggesting that significant contributions of LOOA formation to severe haze pollution in winter.
 320 The contribution of LOOA to OA ranged from 27% to 39% with an average of 34%, and the

321 contribution of MOOA to OA ranged from 26% to 35% with an average of 32%. Overall, the average
322 mass concentration of SOA was about 1.7 times that of POA for the whole year, and SOA accounted
323 for about 32% of NR-PM₁, which was higher than those of sulfate and nitrate, demonstrating the largest
324 contribution of SOA to NR-PM₁.

325 **3.2 Significant contributions of secondary organic aerosols to haze formations in all seasons**

326 Investigations on contribution variations of aerosol compositions under different aerosol pollution
327 levels are helpful for understanding mechanisms of haze formations, and results in four seasons are
328 presented in Fig. 56. The chemical composition of NR-PM₁ under different pollution levels differ much
329 among seasons. In fall, as demonstrated by variations of mass concentrations of aerosol compositions
330 under different pollution levels shown in Fig. 56, pollution conditions in fall were dominantly
331 controlled by secondary formations of sulfate and SOA, accumulation of primary aerosols and nitrate
332 formation had relatively smaller impacts. With respect to mass fractions variations, contributions of
333 aerosol components differed much among different pollution levels. The fraction of OA decreased
334 rapidly from 67% to 50% when the mass concentration of NR-PM₁ gradually increased to 15 μg/m³,
335 while the contribution of sulfate increased substantially from 17% to 30%, and the contribution of
336 nitrate remained relatively stable at about 10%. When NR-PM₁ further increased, OA contribution
337 remained relatively flat for NR-PM₁ below about 50 μg/m³. Accordingly, the contribution of SO₄²⁻
338 decreased to ~18%, and the contribution of nitrate substantially increased from ~10 % to 21%. After
339 that, OA contribution decreased rapidly to about 40% and then remained stable for NR-PM₁ >50 μg/m³.
340 However, the contribution of sulfate began to increase, and the highest contribution could account for
341 30%, while the contribution of nitrate began to decline gradually to 12%. In addition, the SOA
342 contributed dominantly to OA (>60%) for NR-PM₁ > 15 μg/m³ and even reached near 70% for NR-
343 PM₁ > 35 μg/m³, suggesting the dominant role of SOA in OA accumulations in haze events during fall.

344 In winter, haze formations are mostly associated with POA accumulations, SOA and nitrate
345 formations, with nitrate formation playing the most important role, since it is also accompanied by

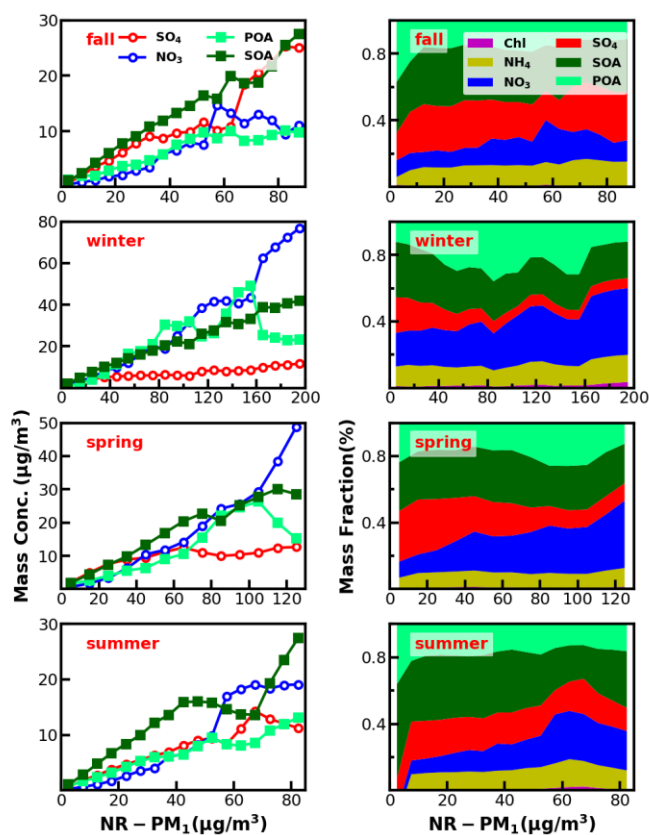


Figure 6. Left panels show absolute mass concentration variations of aerosol compositions under different NR-PM₁ levels, right panels show mass fractions of chemical components as a function of NR-PM₁.

346 ammonium formation, while sulfate formation was weak in winter. The fraction of OA increased
 347 gradually with the increase of NR-PM₁ concentration for NR-PM₁ < 90 µg/m³ and reached the
 348 maximum of 60%, while the contribution of nitrate also showed a small increase from 21% to 26%.
 349 Under aggravating pollution, OA contribution fluctuated, however, showed a decreasing trend from
 350 60% to ~40%. Meanwhile, the nitrate contribution showed an increasing trend from 26% to ~40%,
 351 which was similar to that of OA. Sulfate contribution decreased with the increase of NR-PM₁
 352 concentration for NR-PM₁ < 100 µg/m³ and then remained at about 6% as NR-PM₁ increases. In
 353 addition, the POA contribution increased about 25% to 50% for NR-PM₁ < 100 µg/m³. Overall, the

354 increase of nitrate, POA and SOA together had resulted in severely polluted conditions in winter. The

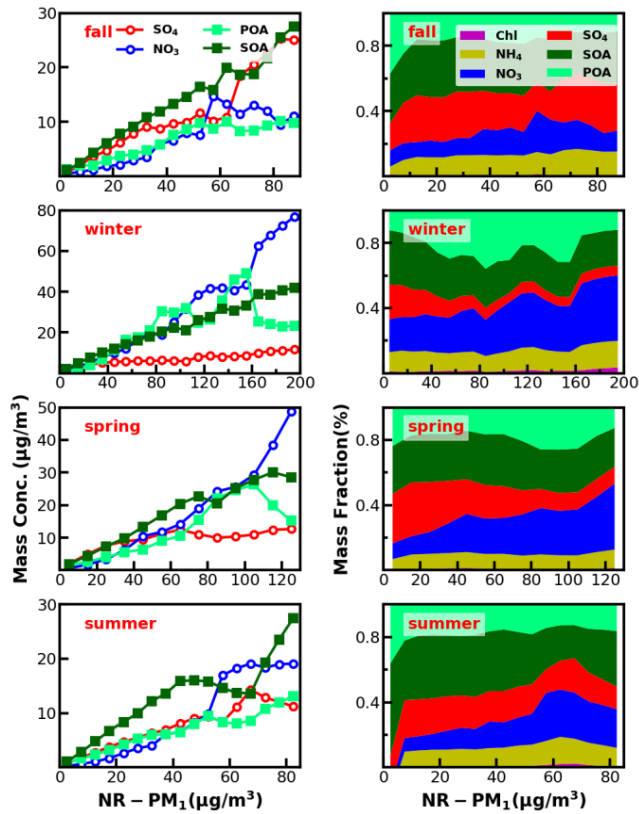


Figure 5. Left panels show absolute mass concentration variations of aerosol compositions under different NR-PM₁ levels, right panels show mass fractions of chemical components as a function of NR-PM₁.

355 substantial contribution of POA to severe haze demonstrates that meteorological conditions
 356 unfavorable for the pollutant diffusion together with the substantial contributions of secondary nitrate
 357 and SOA formations have resulted in the most severe haze pollutions among the year. Especially, HOA
 358 contribution to OA increased from 17% to 52% when NR-PM₁ concentration was less than 140 µg/m³,
 359 suggesting the significant role of traffic emission accumulation during severe haze pollution, which
 360 was consistent with results of Yao et al. (2020).

361 In spring, haze pollutions were mostly associated POA accumulation and secondary formations of
 362 nitrate and SOA, especially that of nitrate. The contribution of OA decreased from 51% to 44% as NR-

363 PM₁ mass concentration increased when NR-PM₁ mass concentration was less than 50 µg/m³. When
364 the mass concentration of NR-PM₁ reached about 105 µg/m³, the fraction of OA reached a maximum
365 of 55%, and then decreased to about 37%. The most noticeable characteristic was the increase of nitrate
366 contribution (from 10% to 40%) and decrease of sulfate contribution (32% to 10%) as the NR-PM₁
367 increased. In summer, secondary aerosol formations contributed dominantly to haze formations, with
368 POA contribution to NR-PM₁ was about 20% in most conditions. The overall contribution of OA
369 gradually decreased from near 60% to 35% as the mass concentration of NR-PM₁ increased for NR-
370 PM₁ concentration < 60 µg/m³ which was markedly different with those in other seasons, however
371 increased to 49% as the NR-PM₁ concentration increased further. The contribution of sulfate decreased
372 from 25% to 13% and the contribution of nitrate increased from 9.0% to 31% with the increase of NR-
373 PM₁ concentration for NR-PM₁ concentration < 60 µg/m³. While the OA was dominated by SOA under
374 most conditions (about 60%).

375 Overall, haze formation mechanisms differed much among distinct seasons. ~~Sulfate mattered more~~
376 ~~than nitrate in fall, while nitrate mattered more than sulfate in spring and winter, however, SOA~~
377 ~~contributed significantly to haze formations in all seasons.~~ Sulfate mattered more than nitrate in fall,
378 while nitrate mattered more than sulfate in spring and winter, however, SOA contributed significantly
379 to haze formations in all seasons. Note that seasonal variations of aerosol chemical compositions might
380 differ much among years due to different meteorological conditions and emissions. For example, the
381 evolution of sulfate during autumn in this study (Fig.S10) have remarkably different accumulation
382 characteristics with those observed in autumn of 2018 as shown in Fig.1 of Chen et al. (2021a). Even
383 so, SOA play significant roles in haze formations of Guangzhou urban area in all seasons hold based
384 on results of existing literatures (Zhou et al., 2020).

386 3.3 Discussions on SOA formation mechanisms

387 ~~SOA can be formed through condensation of oxidized gas phase organic vapors during the~~
388 ~~oxidation of volatile organic compounds (VOCs), this type of formed SOA was usually referred to as~~
389 ~~gasSOA (Kuang et al., 2020). SOA can also be formed in the aqueous phase through the further~~
390 ~~oxidation of dissolved VOCs which are usually products of gas phase oxidation of VOCs, this type of~~

391 SOA was usually referred as aqSOA (Kuang et al., 2020). As shown in Fig.3, both LOOA and MOOA
 392 mainly increased after sunrise, highlighting important roles of photochemistry in SOA formations.
 393 However, as demonstrated by Kuang et al. (2020), the daytime SOA formation could be either result
 394 from gas-phase photochemistry and subsequent condensation (gasSOA), or the result of gas-phase
 395 VOCs transformations with subsequent aqueous reactions (aqSOA). Especially since the PRD region
 396 is characterized by both active photochemistry due to strong solar radiation in subtropical regions and
 397 high relative humidity (annual average RH of ~75%), both photochemistry and aqueous phase
 398 reactions might play significant roles in SOA formation, however, this aspect was not explored before.

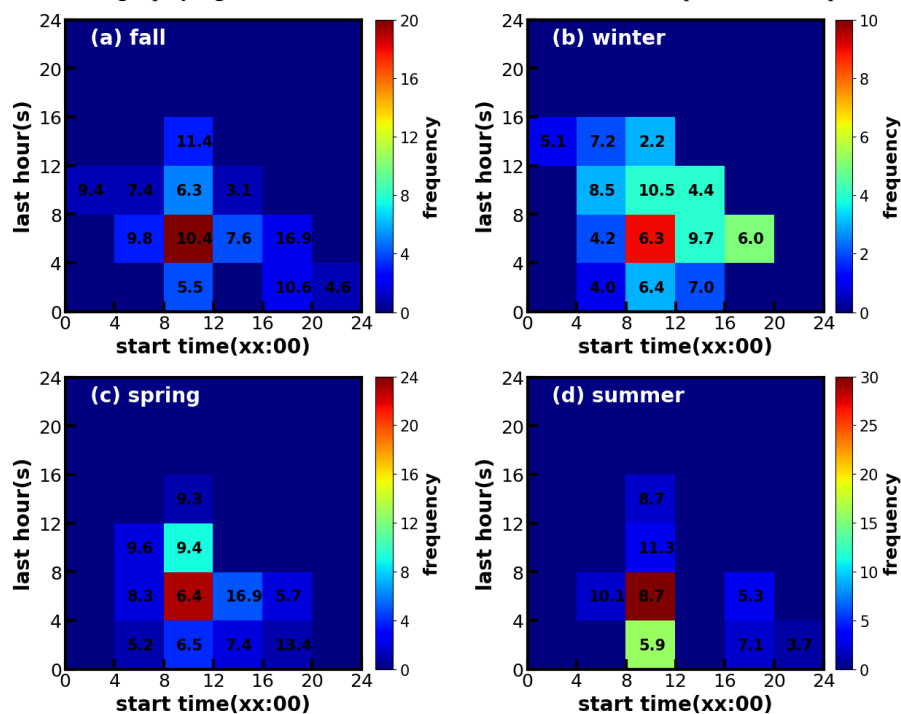


Figure 7. Time frequency diagrams of SOA increase events in (a) fall, (b) winter, (c) spring and (d) summer. X-axis represent start time of SOA increase, and y-axis represents the lasting hours of SOA increase events. The color scales indicate the number of occurrences. The values in the grid are the average SOA concentration during the SOA increase case.

399 Considering the frequent co-increase of MOOA and LOOA, they were grouped together as SOA
 400 for further investigations on their formation. SOA formation cases in four seasons were identified, the
 401 start time and lasting hours of their occurrences, as well as associated SOA levels are shown in Fig. 67.
 402 Note that the identification of SOA formation cases has not considered the dilution effect of the lifting

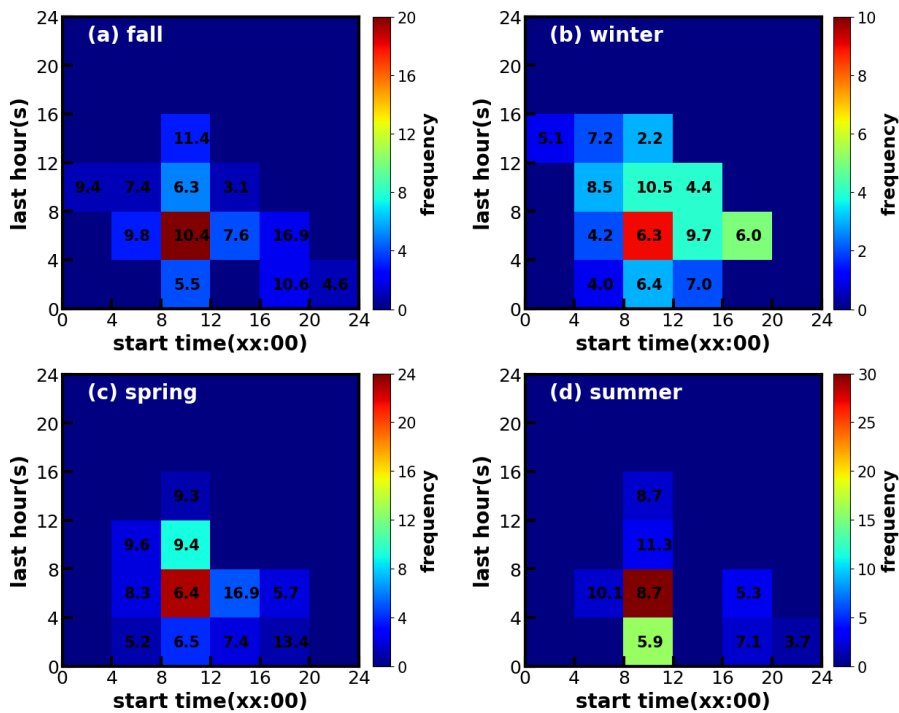


Figure 6: Time-frequency diagrams of SOA increase events in (a) fall, (b) winter, (c) spring and (d) summer. X-axis represent start time of SOA increase, and y-axis represents the lasting hours of SOA increase events. The color scales indicate the number of occurrences. The values in the grid are the average SOA concentration during the SOA increase case.

403 daytime boundary layer height and was only based on the absolute mass concentration variations.
 404 Therefore, this method has neglected some SOA formation cases that were masked by evolutions of
 405 the boundary layer, and the identified cases represent active SOA formation events that overcame
 406 dilution effects, which might be more suitable for further SOA formation investigations due to strong
 407 SOA formation signals. It shows that in all seasons, the SOA formation happened most frequently
 408 during daytime, starting in the morning and lasting about 4-8 hours. Especially, in spring, summer and

409 fall, the daytime SOA formation almost happened everyday (Fig.S5-7), even if strong daytime
410 boundary layer evolutions could be expected in these seasons due to strong surface solar heating, and
411 resulted in the afternoon SOA mass concentration peaks in these seasons (Fig.3). However, highest
412 SOA concentrations did not appear in the seasons with the most frequent morning to afternoon
413 increases. Taking SOA formation cases in spring as an example, if the SOA increase started in the
414 morning, more than 8 hours duration will result in significant higher SOA concentration. These cases
415 started in the afternoon and lasted 4-8 hours would result in highest SOA concentration in spring. The
416 SOA formation cases starting in the morning, however, only lasting within 4 hours, happened
417 frequently in summer while less in spring and fall, suggesting that the absolute SOA mass
418 concentration increase was more often stopped by strong boundary layer mixing in summer, which
419 was consistent with the solar heating characteristics. The highest SOA in fall and winter were
420 associated with the continuous increase of SOA after sunrise, suggesting that coordination of daytime
421 and nighttime SOA formation together had resulted in the highest SOA concentrations in fall and winter.

422 To dig deeper into possible mechanisms behind the active daytime SOA formations throughout
423 the year, we investigated relationships between SOA formation rates and both O₃ as well as aerosol
424 liquid water content (ALWC) for the most frequent morning to afternoon SOA increase cases. Without
425 considering the dilution effect of rising boundary layer, the daytime apparent growth rates of SOA
426 varied from 0.2 to 4.4 μg m⁻³ h⁻¹ (Fig.78). Note that the SOA growth rates was calculated on the basis
427 of observations of the first four hours for each SOA increase case to reduce impacts of boundary layer
428 dilution effects. Some previous studies used variations of CO concentrations to partially correct for
429 boundary layer dilution effects, however this method would fail in sites with strong CO emissions
430 (Kuang et al., 2020). The SOA growth rates and were highly correlated to O₃ formation rates (r=0.7)
431 as shown in Fig.78. However, this result only proved the important role of photochemistry in SOA
432 formations. The apparent SOA growth rates showed positive but much weaker correlation with the
433 average O₃ concentration during the period of SOA the increase (r=0.38), demonstrating that oxidant
434 level was likely not the controlling factor for SOA formation, although O₃ alone did not represent the

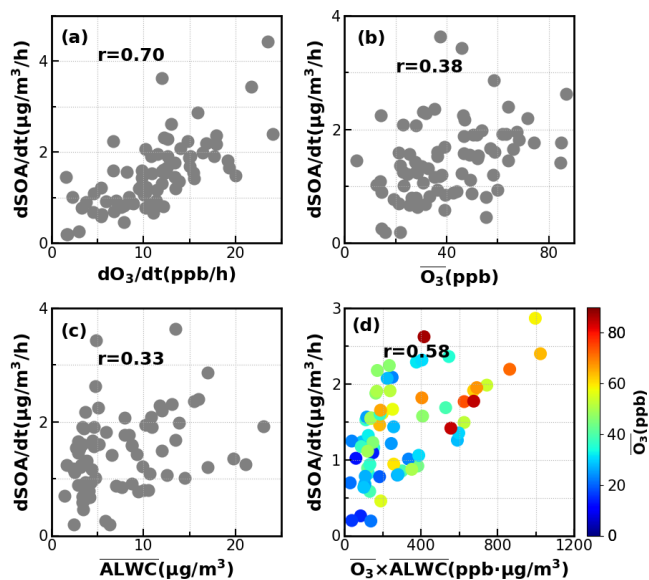


Figure 8. Relationships between SOA daytime formation rates with corresponding (a) O₃ formation rate; (b) average O₃; (c) average ALWC (μg/m³) and (d) combination of averaged O₃ and averaged ALWC.

435 variations of oxidation levels and other sources such as HONO photolysis (Yu et al., 2022) also
 436 contribute to OH radicals and is a typical oxidant in daytime photochemistry. To investigate the
 437 possible roles of aqueous reactions in SOA formation, the relationship between apparent SOA rates
 438 and corresponding average ALWC were also investigated, and a positive but weak correlation was
 439 found (r=0.33). More importantly, the correlation coefficient between apparent SOA growth rates and
 440 the variable of average ALWC multiplying by average O₃ would be much higher (r=0.58, Fig. 7d),
 441 suggesting that the coordination of gas-phase photochemistry and further aqueous reactions had likely
 442 resulted in the rapid daytime SOA formations.

443 Besides the daytime SOA formation associated with photochemistry, dark transformations of
 444 VOCs that involve nighttime gas-phase and aqueous phase reactions might also result in efficient SOA
 445 formations. As shown in Fig.67, continuous increases of SOA were also frequently observed after

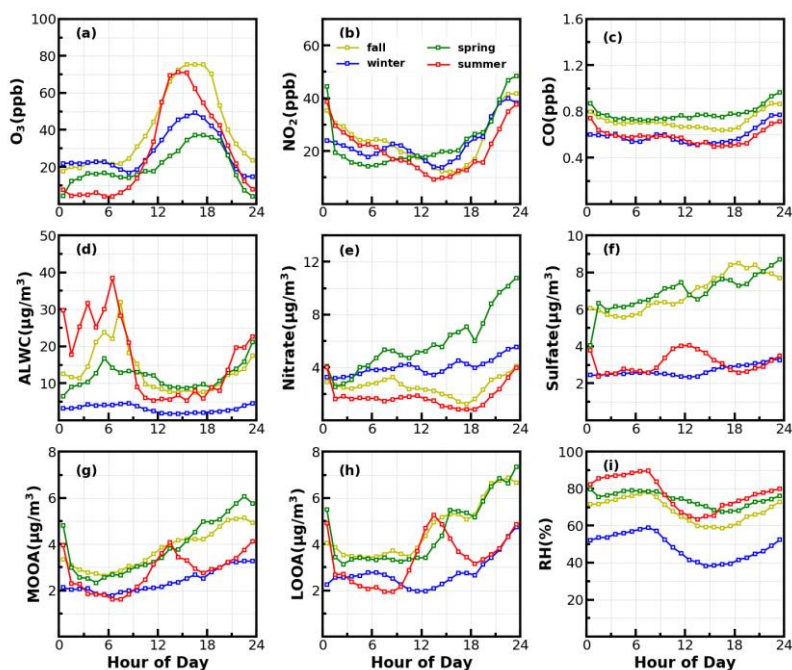


Figure 89. Average diurnal variations of (a) O₃; (b) NO₂; (c) CO; (d) ALWC; (e) nitrate; (f) sulfate; (g) MOOA; (h) LOOA and (i) RH for identified days with nighttime SOA increases.

446 sunset in spring (17 days), fall (18 days) and winter (20 days) with sporadic occurrence in summer,
 447 and the coordination of daytime and nighttime SOA formations together have resulted in the highest
 448 SOA concentrations in fall and winter which were associated with severe haze pollutions as
 449 demonstrated above. Average diurnal profiles of O₃, NO₂, CO, RH, ALWC, nitrate, sulfate, LOOA and
 450 MOOA for cases with co-increases of LOOA and MOOA after 18:00 in different seasons are shown
 451 in Fig.89. On average, SOA usually showed decreases during nighttime (Fig.3) due to transport of air
 452 mass from cleaner suburban regions. The average wind speed was 1.7 m/s from 18:00 to 23:00 LT for
 453 identified nighttime SOA increase cases and was obviously lower than the corresponding average wind
 454 speed of 2.3 m/s, suggesting the more stagnant air mass tended to favor the nighttime SOA increases.

455 However, the nighttime 5h back trajectories shown in Fig. S9S11 demonstrated that the nighttime

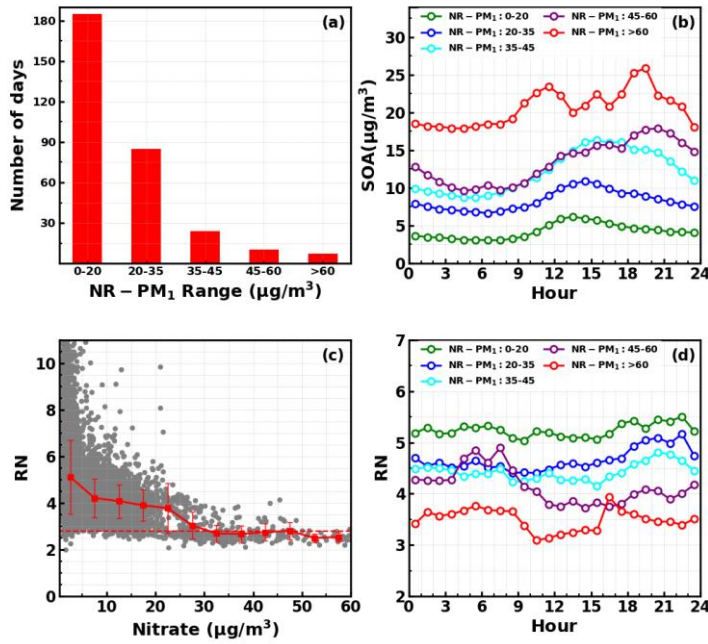


Figure 9. (a) Number of days in different daily average NR-PM₁ ranges; (b) Diurnal profiles of SOA under different NR-PM₁ ranges; (c) Variations NO_x/NO₂+ (RN) as a function of measured nitrate, horizontal dashed line corresponds to RN of 2.8, red markers and bars represents averages and standard deviations; (d) Diurnal profiles of RN under different NR-PM₁ ranges.

456 replacement of surrounding suburban cleaner air mass still prevailed, therefore the continuous
 457 increases of SOA suggested that nighttime SOA formation occurred on a regional scale. The increases
 458 of LOOA and MOOA were accompanied with obvious nitrate formation in all seasons as well as slight
 459 increases of sulfate, further indicating for regional scale nighttime secondary aerosol formations during
 460 these nighttime SOA formation events. Except for summer, continuous increase of SOA from the
 461 morning to nighttime confirmed that the coordination of daytime and nighttime SOA formations had
 462 contributed to haze formations. Number of days for daily average NR-PM₁ ranges of 0-20, 20-35, 35-
 463 45, 45-60 and >60 μg/m³ were 185,85,24,10 and 7, respectively (Fig. 9a10a). All cases with daily

464 average NR-PM₁ higher than 45 μg/m³ occurred in fall, winter and spring. The corresponding average
 465 diurnal variations of SOA for these relatively severe conditions shown in Fig. 9b10b confirmed further
 466 that the coordination of daytime and nighttime SOA formations had contributed to severe haze
 467 formations in Guangzhou urban area.

468 The NO₃ radical formed through the reaction between NO₂ and O₃ is the typical nighttime oxidant.
 469 Results of Rollins et al. (2012) and Kiendler-Scharr et al. (2016) revealed that NO₃ oxidation of VOCs
 470 would contribute substantially to nighttime SOA increase. As shown in Fig. 8a9a, after sunset, the O₃
 471 concentration decreased quickly, however, remained substantially higher than zero, accompanied was
 472 the remarkable increases of NO₂ and nitrate. In Guangzhou urban areas, nitrate can either be formed
 473 through gas-phase oxidation of NO₂ by OH which forms HNO₃ and then condenses onto aerosol phase,
 474 or be formed through the hydrolysis of N₂O₅, which is formed through reactions between NO₂ and

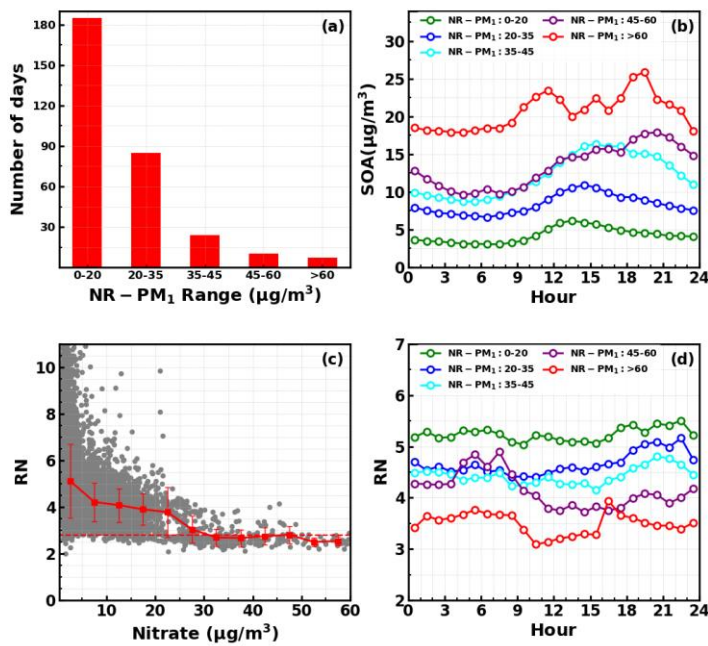


Figure 10. (a) Number of days in different daily average NR-PM₁ ranges; (b) Diurnal profiles of SOA under different NR-PM₁ ranges; (c) Variations NO₃⁻/NO₂⁺ (RN) as a function of measured nitrate, horizontal dashed line corresponds to RN of 2.8, red markers and bars represents averages and standard deviations; (d) Diurnal profiles of RN under different NR-PM₁ ranges.

475 NO₃ radical (Yang et al., 2022). The obvious co-increases in nitrate and SOA after sunset indicated
476 that the decrease of O₃ and increase of NO₂ consumption had supplied the NO₃ and N₂O₅ reaction
477 chains and the increase of ALWC favored the hydrolysis of N₂O₅. This was indirectly confirmed when
478 during winter, despite relatively high concentrations of O₃ and NO₂ after sunrise compared with other
479 seasons, nitrate formation was much less prominent due to substantially lower ALWC associated with
480 lower RH. However, the quick increase of SOA still occurred after sunset despite weak daytime SOA
481 formation, suggesting that aqueous reactions might play minor roles in nighttime SOA formation that
482 involve NO₃ radical in Guangzhou urban area. The nighttime chemistry that involves NO₃ radical
483 might contribute substantially to organic nitrate formation (Ng et al., 2008; Fry et al., 2009; Rollins et
484 al., 2012) which would produce the same ions (NO₃⁺ and NO₂⁺) with inorganic nitrate due to the
485 fragmentation of nitrate functionality (-ONO₂) under 70 eV electron ionization in the aerosol mass
486 spectrometer measurements. However, organic nitrate has different fragmentation pattern with that of
487 inorganic nitrate with previous laboratory studies have shown that the RN=NO₃⁺/NO₂⁺ of organic
488 nitrate is substantially higher than that of inorganic nitrate. Farmer et al. (2010) thus proposed that the
489 RN variations can be used as an indicator of organic nitrate formations. The Q-ACSM measurements
490 with unit mass resolution cannot provide accurate measurements of RN due to the resolution limitation
491 (Allan et al., 2004), however, the resolved RN related to measured nitrate might provide qualitative
492 constraints on impacts of organic nitrates. The variations of resolved RN as a function of measured
493 nitrate are shown in Fig. 9e10c, which shows that at high levels of nitrate when inorganic nitrate usually
494 dominates (Xu et al., 2021), the RN approaches near 2.8 which was close to the inorganic nitrate RN
495 reported in (Xu et al., 2021), and locates in the range of 1.1-3.5 of inorganic nitrate RN reported in
496 literatures (Xu et al., 2015b). Diurnal variations of RN under different pollution levels shown in
497 Fig. 9d (Xu et al., 2015). Diurnal variations of RN under different pollution levels shown in Fig. 10d
498 reveals higher nighttime RN than daytime, and obvious continuous increase of RN after sunset can be
499 observed for relatively clean and polluted conditions (daily average NR-PM₁ of 20-35 μg/m³ to NR-
500 PM₁ of 45-60 μg/m³), suggesting active nighttime organic nitrate formations, which confirmed the
501 involvement of NO₃ radicals in nighttime SOA formations.

设置了格式: 上标

设置了格式: 下标

设置了格式: 上标

设置了格式: 上标

设置了格式: 下标

设置了格式: 上标

4 Implications for future studies

In this study, we highlighted the significant roles of SOA in haze formations in Guangzhou urban area during the entire year and pointed out that for the most prominent and frequent daytime SOA formations all the year around, both gas-phase photochemistry and aqueous reactions played significant roles. Therefore, daytime SOA formation was weak in winter when oxidant level and RH were low, whereas prominent SOA formations were observed in fall, spring and summer on almost daily basis. However, how gas-phase and aqueous phase reactions have coordinated to promote the SOA formation, and the different contributions of gasSOA and aqSOA to SOA formations under different meteorological conditions and VOCs profiles in different seasons are not clear. In addition, our results suggested that the coordination of daytime and nighttime SOA formation together had resulted in highest SOA concentrations in Guangzhou urban area, thus contributed significantly to severe haze formation. The co-increases of nitrate and SOA after sunrise indicated the significant roles of nighttime NO_3 radical chemistry in promoting haze formations. However, our understanding on how nighttime chemistry evolved and contributed to secondary aerosols formations in different seasons is still highly insufficient in this region. Therefore, the precursors and formation pathways of daytime and nighttime SOA formations and how they coordinated to promote severe haze formations need further comprehensive investigations to make targeted emission control strategies to continuously improve air quality in the PRD region. Also, findings of this study have important implications on future investigations of SOA formation mechanisms in urban areas of southern China that share similar emission sources and meteorological conditions.

Data availability. All data needed are presented in time series of Figures and supplementary Figures, raw datasets of this study are available from the corresponding author Li Liu (liul@gd121.cn) upon request.

Competing interests. The authors declare that they have no conflict of interest.

Author Contributions. YK and LL designed the aerosol experiments. YK conceived and led this research. MMZ and YK wrote the manuscript. MMZ and LL conducted the long-term Q-ACSM

531 measurements. MMZ and YH performed the PMF analysis. HBX, CY, YZ and FL helped maintain and
532 calibrating the Q-ACSM. CL provided meteorological datasets, BL performed the AE33 measurements
533 and post data processing. XJD obtained funding for the continuous aerosol measurements. JCT and
534 WYX provided insights into data analysis, and all authors contributed to revisions of this paper.

535
536

537 **Acknowledgments**

538 This work is supported by the Guangdong Provincial Key Research and Development Program
539 (2020B1111360003); National Natural Science Foundation of China (42175083 and 42105092);
540 Guangdong Basic and Applied Basic Research Foundation (2019A1515110791 and
541 2019A1515011808); National Key Research and Development Program of China (2019YFCO214605);
542 Science and Technology Innovation Team Plan of Guangdong Meteorological Bureau
543 (GRMCTD202003). The Special Fund Project for Science and Technology Innovation Strategy of
544 Guangdong Province (Grant No.2019B121205004).

545

546 **References**

547 Allan, J. D., Delia, A. E., Coe, H., Bower, K. N., Alfarra, M. R., Jimenez, J. L., Middlebrook, A. M., Drewnick, F., Onasch,
548 T. B., Canagaratna, M. R., Jayne, J. T., and Worsnop, D. R.: A generalised method for the extraction of chemically
549 resolved mass spectra from Aerodyne aerosol mass spectrometer data, *Journal of Aerosol Science*, 35, 909–922,
550 <https://doi.org/10.1016/j.jaerosci.2004.02.007><https://doi.org/10.1016/j.jaerosci.2004.02.007>, 2004.
551 ~~Allan, J. D., Williams, P. I., Morgan, W. T., Martin, C. L., Flynn, M. J., Lee, J., Nemitz, E., Phillips, G. J., Gallagher, M. W.,
552 and Coe, H.: Contributions from transport, solid fuel burning and cooking to primary organic aerosols in two UK
553 cities, *Atmospheric Chemistry and Physics*, 10, 647–668, [10.5194/acp-10-647-2010](https://doi.org/10.5194/acp-10-647-2010), 2010.~~
554 Canagaratna, M. R., Jayne, J. T., Jimenez, J. L., Allan, J. D., Alfarra, M. R., Zhang, Q., Onasch, T. B., Drewnick, F., Coe,
555 H., Middlebrook, A., Delia, A., Williams, L. R., Trimborn, A. M., Northway, M. J., DeCarlo, P. F., Kolb, C. E., Davidovits,
556 P., and Worsnop, D. R.: Chemical and microphysical characterization of ambient aerosols with the aerodyne aerosol
557 mass spectrometer, *Mass Spectrom Rev*, 26, 185–222, [10.1002/mas.20115](https://doi.org/10.1002/mas.20115), 2007.
558 Canonaco, F., Crippa, M., Slowik, J. G., Baltensperger, U., and Prevot, A. S. H.: SoFi, an IGOR-based interface for the
559 efficient use of the generalized multilinear engine (ME-2) for the source apportionment: ME-2 application to
560 aerosol mass spectrometer data, *Atmos. Meas. Tech.*, 6, 3649–3661, [10.5194/amt-6-3649-2013](https://doi.org/10.5194/amt-6-3649-2013), 2013.
561 Canonaco, F., Tobler, A., Chen, G., Sosedova, Y., Slowik, J. G., Bozzetti, C., Daellenbach, K. R., El Haddad, I., Crippa,
562 M., Huang, R. J., Furger, M., Baltensperger, U., and [PrevotPrévôt](https://doi.org/10.5194/amt-6-3649-2013), A. S. H.: A new method for long-term source

563 apportionment with time-dependent factor profiles and uncertainty assessment using SoFi Pro: application to 1
564 year of organic aerosol data, *Atmos. Meas. Tech.*, 14, 923–943, 10.5194/amt-14-923-2021, 2021.

565 [Chen, W., Ye, Y., Hu, W., Zhou, H., Pan, T., Wang, Y., Song, W., Song, Q., Ye, C., Wang, C., Wang, B., Huang, S., Yuan,](#)
566 [B., Zhu, M., Lian, X., Zhang, G., Bi, X., Jiang, F., Liu, J., Canonaco, F., Prevot, A. S. H., Shao, M., and Wang, X.: Real-](#)
567 [Time Characterization of Aerosol Compositions, Sources, and Aging Processes in Guangzhou During PRIDE-GBA](#)
568 [2018 Campaign, *Journal of Geophysical Research: Atmospheres*, 126, e2021JD035114, 2021a,](#)
569 <https://doi.org/10.1029/2021JD035114>.

570 [Chen, W., Ye, Y. Q., Hu, W. W., Zhou, H. S., Pan, T. L., Wang, Y. K., Song, W., Song, Q. C., Ye, C. S., Wang, C. M.,](#)
571 [Wang, B. L., Huang, S., Yuan, B., Zhu, M., Lian, X. F., Zhang, G. H., Bi, X. H., Jiang, F., Liu, J. W., Canonaco, F., Prevot,](#)
572 [A. S. H., Shao, M., and Wang, X. M.: Real-Time Characterization of Aerosol Compositions, Sources, and Aging](#)
573 [Processes in Guangzhou During PRIDE-GBA 2018 Campaign, *J Geophys Res-Atmos*, 126, ARTN e2021JD035114](#)
574 [10.1029/2021JD035114](https://doi.org/10.1029/2021JD035114), 2021b.

575 Drinovec, L., Močnik, G., Zotter, P., Prévôt, A. S. H., Ruckstuhl, C., Coz, E., Rupakheti, M., Sciare, J., Müller, T.,
576 Wiedensohler, A., and Hansen, A. D. A.: The "dual-spot" Aethalometer: an improved measurement of aerosol black
577 carbon with real-time loading compensation, *Atmospheric Measurement Techniques*, 8, 1965–1979, 10.5194/amt-
578 8-1965-2015, 2015.

579 [Ervens, B., Turpin, B. J., and Weber, R. J.: Secondary organic aerosol formation in cloud droplets and aqueous](#)
580 [particles \(aqSOA\): a review of laboratory, field and model studies, *Atmos. Chem. Phys.*, 11, 11069–11102,](#)
581 [10.5194/acp-11-11069-2011](https://doi.org/10.5194/acp-11-11069-2011), 2011.

582 Farmer, D. K., Matsunaga, A., Docherty, K. S., Surratt, J. D., Seinfeld, J. H., Ziemann, P. J., and Jimenez, J. L.: Response
583 of an aerosol mass spectrometer to organonitrates and organosulfates and implications for atmospheric chemistry,
584 *Proceedings of the National Academy of Sciences*, 107, 6670–6675, doi:10.1073/pnas.0912340107, 2010.

585 [Fröhlich, R., Cubison, M. J., Slowik, J. G., Bukowiecki, N., Prévôt, A. S. H., Baltensperger, U., Schneider, J., Kimmel, J.,](#)
586 [R., Gonin, M., Rohner, U., Worsnop, D. R., and Jayne, J. T.: The ToF-ACSM: a portable aerosol chemical speciation](#)
587 [monitor with TOFMS detection, *Atmos. Meas. Tech.*, 6, 3225–3241, 10.5194/amt-6-3225-2013](#), 2013.

588 Fry, J. L., Kiendler-Scharr, A., Rollins, A. W., Wooldridge, P. J., Brown, S. S., Fuchs, H., Dubé, W., Mensah, A., dal Maso,
589 M., Tillmann, R., Dorn, H. P., Brauers, T., and Cohen, R. C.: Organic nitrate and secondary organic aerosol yield from
590 NO₃ oxidation of β-pinene evaluated using a gas-phase kinetics/aerosol partitioning model, *Atmos.*
591 *Chem. Phys.*, 9, 1431–1449, 10.5194/acp-9-1431-2009, 2009.

592 Guo, H., Liu, J., Froyd, K. D., Roberts, J. M., Veres, P. R., Hayes, P. L., Jimenez, J. L., Nenes, A., and Weber, R. J.: Fine
593 particle pH and gas–particle phase partitioning of inorganic species in Pasadena, California, during the 2010 CalNex
594 campaign, *Atmospheric Chemistry and Physics*, 17, 5703–5719, 10.5194/acp-17-5703-2017, 2017.

595 Guo, J. C., Zhou, S. Z., Cai, M. F., Zhao, J., Song, W., Zhao, W. X., Hu, W. W., Sun, Y. L., He, Y., Yang, C. Q., Xu, X. Z.,
596 Zhang, Z. S., Cheng, P., Fan, Q., Hang, J., Fan, S. J., Wang, X. M., and Wang, X. M.: Characterization of submicron
597 particles by time-of-flight aerosol chemical speciation monitor (ToF-ACSM) during wintertime: aerosol
598 composition, sources, and chemical processes in Guangzhou, China, *Atmospheric Chemistry and Physics*, 20, 7595–
599 7615, 10.5194/acp-20-7595-2020, 2020.

600 He, L. Y., Huang, X. F., Xue, L., Hu, M., Lin, Y., Zheng, J., Zhang, R. Y., and Zhang, Y. H.: Submicron aerosol analysis
601 and organic source apportionment in an urban atmosphere in Pearl River Delta of China using high-resolution
602 aerosol mass spectrometry, *J Geophys Res-Atmos*, 116, Artn D12304
603 [10.1029/2010jd014566](https://doi.org/10.1029/2010jd014566), 2011.

604 [HuHuang, X., Ding, A., Gao, J., Zheng, B., Zhou, D., Qi, X., Tang, R., Wang, J., Ren, C., Nie, W., Chi, X., Xu, Z., Chen,](#)
605 [L., Li, Y., Che, F., Pang, N., Wang, H., Tong, D., Qin, W., Hu, M., HuCheng, W., Jimenez, J. L., Yuan, B., Chen, Liu, W,](#)
606 [T., Wang, M., Wu, Y. S., Chen, C., Wang, Z., Fu, Q., Liu, B., Peng, J. F., Zeng, L. M., and Shao, M.: Chemical composition,](#)

607 [sources, and aging process of submicron aerosols in Beijing: Contrast between summer and winter](#), *J Geophys Res-*
608 *Atmos*, **121**, 1955–1977, [10.1002/2015jd024020](#), 2016.

609 [Huang, R., Chai, F., Davis, S. J., Zhang, Y., Bozzetti, C., He, Q., and He, K. F., Cao, J. J., Han, Y., Daellenbach, K. R., Slowik,](#)
610 [J. G., Platt, S. M., Canonaco, F., Zotter, P., Wolf, R., Pieber, S. M., Bruns, E. A., Crippa, M., Ciarelli, G., Piazzalunga, A.,](#)
611 [Schwikowski, M., Abbazade, G., Schnelle-Kreis, J., Zimmermann, R., An, Z., Szidat, S., Baltensperger, U., El Haddad,](#)
612 [I., and Prevot, A. S.: High.: Enhanced secondary aerosol contribution to particulate pollution offset reduction of](#)
613 [primary emissions during haze events COVID-19 lockdown in China](#), *Nature*, **514**, 218–222, [10.1038/nature13774](#),

614 [2014](#) *National Science Review*, **8**, nwa137, [10.1093/nsr/nwaa137](#), 2021.

615 Huang, X. F., He, L. Y., Hu, M., Canagaratna, M. R., Kroll, J. H., Ng, N. L., Zhang, Y. H., Lin, Y., Xue, L., Sun, T. L., Liu, X.
616 G., Shao, M., Jayne, J. T., and Worsnop, D. R.: Characterization of submicron aerosols at a rural site in Pearl River
617 Delta of China using an Aerodyne High-Resolution Aerosol Mass Spectrometer, *Atmospheric Chemistry and Physics*,
618 **11**, 1865–1877, [10.5194/acp-11-1865-2011](#), 2011.

619 Jayne, J. T., Leard, D. C., Zhang, X. F., Davidovits, P., Smith, K. A., Kolb, C. E., and Worsnop, D. R.: Development of an
620 aerosol mass spectrometer for size and composition analysis of submicron particles, *Aerosol Science and*
621 *Technology*, **33**, 49–70, [Doi 10.1080/027868200410840](#), 2000.

622 Jimenez, J. L., Jayne, J. T., Shi, Q., Kolb, C. E., Worsnop, D. R., Yourshaw, I., Seinfeld, J. H., Flagan, R. C., Zhang, X. F.,
623 Smith, K. A., Morris, J. W., and Davidovits, P.: Ambient aerosol sampling using the Aerodyne Aerosol Mass
624 Spectrometer, *J Geophys Res-Atmos*, **108**, Artn 8425
625 [10.1029/2001jd001213](#), 2003.

626 Jimenez, J. L., Canagaratna, M. R., Donahue, N. M., Prevot, A. S. H., Zhang, Q., Kroll, J. H., DeCarlo, P. F., Allan, J. D.,
627 Coe, H., Ng, N. L., Aiken, A. C., Docherty, K. S., Ulbrich, I. M., Grieshop, A. P., Robinson, A. L., Duplissy, J., Smith, J. D.,
628 Wilson, K. R., Lanz, V. A., Hueglin, C., Sun, Y. L., Tian, J., Laaksonen, A., Raatikainen, T., Rautiainen, J., Vaattovaara, P.,
629 Ehn, M., Kulmala, M., Tomlinson, J. M., Collins, D. R., Cubison, M. J., Dunlea, J., Huffman, J. A., Onasch, T. B., Alfarra,
630 M. R., Williams, P. I., Bower, K., Kondo, Y., Schneider, J., Drewnick, F., Borrmann, S., Weimer, S., Demerjian, K., Salcedo,
631 D., Cottrell, L., Griffin, R., Takami, A., Miyoshi, T., Hatakeyama, S., Shimono, A., Sun, J. Y., Zhang, Y. M., Dzepina, K.,
632 Kimmel, J. R., Sueper, D., Jayne, J. T., Herndon, S. C., Trimborn, A. M., Williams, L. R., Wood, E. C., Middlebrook, A.
633 M., Kolb, C. E., Baltensperger, U., and Worsnop, D. R.: Evolution of Organic Aerosols in the Atmosphere, *Science*,
634 **326**, 1525–1529, [10.1126/science.1180353](#), 2009.

635 Kiendler-Scharr, A., Mensah, A. A., Friese, E., Topping, D., Nemitz, E., Prevot, A. S. H., Äijälä, M., Allan, J., Canonaco,
636 F., Canagaratna, M., Carbone, S., Crippa, M., Dall'Osto, M., Day, D. A., De Carlo, P., Di Marco, C. F., Elbern, H., Eriksson,
637 A., Freney, E., Hao, L., Herrmann, H., Hildebrandt, L., Hillamo, R., Jimenez, J. L., Laaksonen, A., McFiggans, G., Mohr,
638 C., O'Dowd, C., Otjes, R., Ovadnevaite, J., Pandis, S. N., Poulain, L., Schlag, P., Sellegri, K., Swietlicki, E., Tiitta, P.,
639 Vermeulen, A., Wahner, A., Worsnop, D., and Wu, H.-C.: Ubiquity of organic nitrates from nighttime chemistry in
640 the European submicron aerosol, *Geophysical Research Letters*, **43**, 7735–7744, [10.1002/2016gl069239](#), 2016.

641 Kuang, Y., He, Y., Xu, W., Yuan, B., Zhang, G., Ma, Z., Wu, C., Wang, C., Wang, S., Zhang, S., Tao, J., Ma, N., Su, H.,
642 Cheng, Y., Shao, M., and Sun, Y.: Photochemical Aqueous-Phase Reactions Induce Rapid Daytime Formation of
643 Oxygenated Organic Aerosol on the North China Plain, *Environmental science & technology*, **54**, 3849–3860,
644 [10.1021/acs.est.9b06836](#), 2020.

645 [Lei, L., Sun, Y., Ouyang, B., Qiu, Y., Xie, C., Tang, G., Zhou, W., He, Y., Wang, Q., Cheng, X., Fu, P., and Wang, Z.:](#)
646 [Vertical Distributions of Primary and Secondary Aerosols in Urban Boundary Layer: Insights into Sources, Chemistry,](#)
647 [and Interaction with Meteorology](#), *Environmental science & technology*, **55**, 4542–4552, [10.1021/acs.est.1c00479](#),

648 [2021](#).

649 Li, Y. J., Lee, B. P., Su, L., Fung, J. C. H., and Chan, C. K.: Seasonal characteristics of fine particulate matter (PM) based
650 on high-resolution time-of-flight aerosol mass spectrometric (HR-ToF-AMS) measurements at the HKUST

651 Supersite in Hong Kong, *Atmos. Chem. Phys.*, 15, 37-53, 10.5194/acp-15-37-2015, 2015.

652 Li, Z., Lei, L., Li, Y., Chen, C., Wang, Q., Zhou, W., Sun, J., Xie, C., and Sun, Y.: Aerosol characterization in a city in
653 central China plain and implications for emission control, *J Environ Sci (China)*, 104, 242-252,
654 10.1016/j.jes.2020.11.015, 2021.

655 Liu, L., Kuang, Y., Zhai, M., Xue, B., He, Y., Tao, J., Luo, B., Xu, W., Tao, J., Yin, C., Li, F., Xu, H., Deng, T., Deng, X., Tan,
656 H., and Shao, M.: Strong light scattering of highly oxygenated organic aerosols impacts significantly on visibility
657 degradation, *Atmos. Chem. Phys.*, 22, 7713-7726, 10.5194/acp-22-7713-2022, 2022.

658 Middlebrook, A. M., Bahreini, R., Jimenez, J. L., and Canagaratna, M. R.: Evaluation of Composition-Dependent
659 Collection Efficiencies for the Aerodyne Aerosol Mass Spectrometer using Field Data, *Aerosol Science and
660 Technology*, 46, 258-271, 10.1080/02786826.2011.620041, 2012.

661 Mohr, C., DeCarlo, P. F., Heringa, M. F., Chirico, R., Slowik, J. G., Richter, R., Reche, C., Alastuey, A., Querol, X., Seco,
662 R., Penuelas, J., Jimenez, J. L., Crippa, M., Zimmermann, R., Baltensperger, U., and Prevot, A. S. H.: Identification and
663 quantification of organic aerosol from cooking and other sources in Barcelona using aerosol mass spectrometer
664 data, *Atmospheric Chemistry and Physics*, 12, 1649-1665, 10.5194/acp-12-1649-2012, 2012.

665 Ng, N. L., Kwan, A. J., Surratt, J. D., Chan, A. W. H., Chhabra, P. S., Sorooshian, A., Pye, H. O. T., Crouse, J. D.,
666 Wennberg, P. O., Flagan, R. C., and Seinfeld, J. H.: Secondary organic aerosol (SOA) formation from reaction of
667 isoprene with nitrate radicals (NO_3), *Atmos. Chem. Phys.*, 8, 4117-4140, 10.5194/acp-8-4117-2008,
668 2008.

669 Ng, N. L., Herndon, S. C., Trimborn, A., Canagaratna, M. R., Croteau, P. L., Onasch, T. B., Sueper, D., Worsnop, D. R.,
670 Zhang, Q., Sun, Y. L., and Jayne, J. T.: An Aerosol Chemical Speciation Monitor (ACSM) for Routine Monitoring of
671 the Composition and Mass Concentrations of Ambient Aerosol, *Aerosol Science and Technology*, 45, 780-794, Pii
672 934555189
673 10.1080/02786826.2011.560211, 2011.

674 Paatero, P.: The Multilinear Engine—A Table-Driven, Least Squares Program for Solving Multilinear Problems,
675 Including then-Way Parallel Factor Analysis Model, *Journal of Computational and Graphical Statistics*, 8, 854-888,
676 10.1080/10618600.1999.10474853, 1999.

677 Qin, Y. M., Tan, H. B., Li, Y. J., Schurman, M. I., Li, F., Canonaco, F., Prevot, A. S. H., and Chan, C. K.: Impacts of traffic
678 emissions on atmospheric particulate nitrate and organics at a downwind site on the periphery of Guangzhou,
679 China, *Atmospheric Chemistry and Physics*, 17, 10245-10258, 10.5194/acp-17-10245-2017, 2017.

680 Rollins, A. W., Browne, E. C., Min, K. E., Pusede, S. E., Wooldridge, P. J., Gentner, D. R., Goldstein, A. H., Liu, S., Day,
681 D. A., Russell, L. M., and Cohen, R. C.: Evidence for NO_3 Control over
682 Nighttime SOA Formation, *Science*, 337, 1210, 10.1126/science.1221520, 2012.

683 [Su, H., Cheng, Y., and Pöschl, U.: New Multiphase Chemical Processes Influencing Atmospheric Aerosols, Air Quality,
684 and Climate in the Anthropocene, *Accounts of chemical research*, 53, 2034-2043, 10.1021/acs.accounts.0c00246,
685 2020.](#)

686 Sun, Y., Du, W., Fu, P., Wang, Q., Li, J., Ge, X., Zhang, Q., Zhu, C., Ren, L., Xu, W., Zhao, J., Han, T., Worsnop, D. R.,
687 and Wang, Z.: Primary and secondary aerosols in Beijing in winter: sources, variations and
688 processes, *Atmospheric Chemistry and Physics*, *Atmos. Chem. Phys.*, 16, 8309-8329, 10.5194/acp-16-8309-2016,
689 2016.

690 Sun, Y. L., Zhang, Q., Schwab, J. J., Demerjian, K. L., Chen, W. N., Bae, M. S., Hung, H. M., Hogrefe, O., Frank, B.,
691 Rattigan, O. V., and Lin, Y. C.: Characterization of the sources and processes of organic and inorganic aerosols in
692 New York city with a high-resolution time-of-flight aerosol mass spectrometer, *Atmospheric Chemistry and Physics*,
693 11, 1581-1602, 10.5194/acp-11-1581-2011, 2011.

694 Sun, Y. L., Wang, Z. F., Dong, H. B., Yang, T., Li, J., Pan, X. L., Chen, P., and Jayne, J. T.: Characterization of summer

695 organic and inorganic aerosols in Beijing, China with an Aerosol Chemical Speciation Monitor, *Atmos. Environ.*, 51,
696 250-259, [10.1016/j.atmosenv.2012.01.013](https://doi.org/10.1016/j.atmosenv.2012.01.013), 2012.

697 Sun, Y. L., Wang, Z. F., Fu, P. Q., Yang, T., Jiang, Q., Dong, H. B., Li, J., and Jia, J. J.: Aerosol composition, sources and
698 processes during wintertime in Beijing, China, *Atmospheric Chemistry and Physics*, 13, 4577-4592, [10.5194/acp-](https://doi.org/10.5194/acp-13-4577-2013)
699 [13-4577-2013](https://doi.org/10.5194/acp-13-4577-2013), 2013.

700 Sun, Y. L., Jiang, Q., Wang, Z. F., Fu, P. Q., Li, J., Yang, T., and Yin, Y.: Investigation of the sources and evolution
701 processes of severe haze pollution in Beijing in January 2013, *J Geophys Res Atmos*, 119, 4380-4398,
702 [10.1002/2014jd021641](https://doi.org/10.1002/2014jd021641), 2014.

703 Sun, Y. L., Wang, Z. F., Du, W., Zhang, Q., Wang, Q. Q., Fu, P. Q., Pan, X. L., Li, J., Jayne, J., and Worsnop, D. R.: Long -
704 term real-time measurements of aerosol particle composition in Beijing, China: seasonal variations, meteorological
705 effects, and source analysis, *Atmospheric Chemistry and Physics*, 15, 10149-10165, [10.5194/acp-15-10149-2015](https://doi.org/10.5194/acp-15-10149-2015),
706 2015.

707 Sun, Y. L., Xu, W. Q., Zhang, Q., Jiang, Q., Canonaco, F., Preevot, A. S. H., Fu, P. Q., Li, J., Jayne, J., Worsnop, D. R.,
708 and Wang, Z. F.: Source apportionment of organic aerosol from 2-year highly time-resolved measurements by an
709 aerosol chemical speciation monitor in Beijing, China, *Atmospheric Chemistry and Physics*, 18, 8469-8489,
710 [10.5194/acp-18-8469-2018](https://doi.org/10.5194/acp-18-8469-2018), 2018.

711 Ulbrich, I. M., Canagaratna, M. R., Zhang, Q., Worsnop, D. R., and Jimenez, J. L.: Interpretation of organic
712 components from Positive Matrix Factorization of aerosol mass spectrometric data, *Atmospheric Chemistry and*
713 *Physics*, 9, 2891-2918, [10.5194/acp-9-2891-2009](https://doi.org/10.5194/acp-9-2891-2009), 2009.

714 Via, M., Minguillón, M. C., Reche, C., Querol, X., and Alastuey, A.: Increase in secondary organic aerosol in an urban
715 environment, *Atmospheric Chemistry and Physics*, 21, 8323-8339, [10.5194/acp-21-8323-2021](https://doi.org/10.5194/acp-21-8323-2021), 2021.

716 Xu, L., Guo, H., Boyd, C. M., Klein, M., Bougiatioti, A., Cerully, K. M., Hite, J. R., Isaacman-VanWertz, G., Kreisberg, N.
717 M., Knote, C., Olson, K., Koss, A., Goldstein, A. H., Hering, S. V., de Gouw, J., Baumann, K., Lee, S. H., Nenes, A.,
718 Weber, R. J., and Ng, N. L.: Effects of anthropogenic emissions on aerosol formation from isoprene and
719 monoterpenes in the southeastern United States, *Proc Natl Acad Sci U S A*, 112, 37-42, [10.1073/pnas.1417609112](https://doi.org/10.1073/pnas.1417609112),
720 2015a.

721 Xu, L., Suresh, S., Guo, H., Weber, R. J., and Ng, N. L.: Aerosol characterization over the southeastern United States
722 using high-resolution aerosol mass spectrometry: spatial and seasonal variation of aerosol composition and sources
723 with a focus on organic nitrates, *Atmos. Chem. Phys.*, 15, 7307-7336, [10.5194/acp-15-7307-2015](https://doi.org/10.5194/acp-15-7307-2015), [2015b](https://doi.org/10.5194/acp-15-7307-2015), 2015.

724 Xu, W., Kuang, Y., Bian, Y., Liu, L., Li, F., Wang, Y., Xue, B., Luo, B., Huang, S., Yuan, B., Zhao, P., and Shao, M.: Current
725 Challenges in Visibility Improvement in Southern China, *Environmental Science & Technology Letters*, 7, 395-401,
726 [10.1021/acs.estlett.0c00274](https://doi.org/10.1021/acs.estlett.0c00274), 2020.

727 Xu, W., Takeuchi, M., Chen, C., Qiu, Y., Xie, C., Xu, W., Ma, N., Worsnop, D. R., Ng, N. L., and Sun, Y.: Estimation of
728 particulate organic nitrates from thermodenuder-aerosol mass spectrometer measurements in the North China
729 Plain, *Atmos. Meas. Tech.*, 14, 3693-3705, [10.5194/amt-14-3693-2021](https://doi.org/10.5194/amt-14-3693-2021), 2021.

730 Yang, D., Li, C., Lau, A. K. H., and Li, Y.: Long-term measurement of daytime atmospheric mixing layer height over
731 Hong Kong, *Journal of Geophysical Research*, 118, 2422-2433, 2013.

732 Yang, S., Yuan, B., Peng, Y., Huang, S., Chen, W., Hu, W., Pei, C., Zhou, J., Parrish, D. D., Wang, W., He, X., Cheng, C.,
733 Li, X. B., Yang, X., Song, Y., Wang, H., Qi, J., Wang, B., Wang, C., Wang, C., Wang, Z., Li, T., Zheng, E., Wang, S., Wu,
734 C., Cai, M., Ye, C., Song, W., Cheng, P., Chen, D., Wang, X., Zhang, Z., Wang, X., Zheng, J., and Shao, M.: The
735 formation and mitigation of nitrate pollution: comparison between urban and suburban environments, *Atmos.*
736 *Chem. Phys.*, 22, 4539-4556, [10.5194/acp-22-4539-2022](https://doi.org/10.5194/acp-22-4539-2022), 2022.

737 Yao, T., Li, Y., Gao, J., Fung, J. C. H., Wang, S., Li, Y., Chan, C. K., and Lau, A. K. H.: Source apportionment of secondary
738 organic aerosols in the Pearl River Delta region: Contribution from the oxidation of semi-volatile and intermediate

739 volatility primary organic aerosols, *Atmospheric Environment*, 222, 117111, 10.1016/j.atmosenv.2019.117111, 2020.

740 Yu, Y., Cheng, P., Li, H., Yang, W., Han, B., Song, W., Hu, W., Wang, X., Yuan, B., Shao, M., Huang, Z., Li, Z., Zheng, J.,

741 Wang, H., and Yu, X.: Budget of nitrous acid (HONO) at an urban site in the fall season of Guangzhou, China, *Atmos.*

742 *Chem. Phys.*, 22, 8951-8971, 10.5194/acp-22-8951-2022, 2022.

743 Zhang, Q., Jimenez, J. L., Canagaratna, M. R., Allan, J. D., Coe, H., Ulbrich, I., Alfarra, M. R., Takami, A., Middlebrook,

744 A. M., Sun, Y. L., Dzepina, K., Dunlea, E., Docherty, K., DeCarlo, P. F., Salcedo, D., Onasch, T., Jayne, J. T., Miyoshi, T.,

745 Shimono, A., Hatakeyama, S., Takegawa, N., Kondo, Y., Schneider, J., Drewnick, F., Borrmann, S., Weimer, S.,

746 Demerjian, K., Williams, P., Bower, K., Bahreini, R., Cottrell, L., Griffin, R. J., Rautiainen, J., Sun, J. Y., Zhang, Y. M., and

747 Worsnop, D. R.: Ubiquity and dominance of oxygenated species in organic aerosols in anthropogenically-influenced

748 Northern Hemisphere midlatitudes, *Geophysical Research Letters*, 34, n/a-n/a, 10.1029/2007GL029979, 2007.

749 Zhang, Q., Jimenez, J. L., Canagaratna, M. R., Ulbrich, I. M., Ng, N. L., Worsnop, D. R., and Sun, Y.: Understanding

750 atmospheric organic aerosols via factor analysis of aerosol mass spectrometry: a review, *Analytical and Bioanalytical*

751 *Chemistry*, 401, 3045-3067, 10.1007/s00216-011-5355-y, 2011.

752 ~~Zhang, Y., Sun, J., Zhang, X., Shen, X., Wang, T., and Qin, M.: Seasonal characterization of components and size~~

753 ~~distributions for submicron aerosols in Beijing, *Science China Earth Sciences*, 56, 890-900, 10.1007/s11430-012-~~

754 ~~4515-z, 2012.~~

755 ~~Zhang, Y.~~ J., Tang, L. L., Wang, Z., Yu, H. X., Sun, Y. L., Liu, D., Qin, W., Canonaco, F., Prevot, A. S. H., Zhang, H. L.,

756 and Zhou, H. C.: Insights into characteristics, sources, and evolution of submicron aerosols during harvest seasons

757 in the Yangtze River delta region, China, *Atmospheric Chemistry and Physics*, 15, 1331-1349, 10.5194/acp-15-

758 1331-2015, 2015.

759 ~~Zhao, J., Qiu, Y., Zhou, W., Xu, W., Wang, J., Zhang, Y., Li, L., Xie, C., Wang, Q., Du, W., Worsnop, D. R., Canagaratna,~~

760 ~~M. R., Zhou, L., Ge, X., Fu, P., Li, J., Wang, Z., Donahue, N. M., and Sun, Y.: Organic Aerosol Processing During Winter~~

761 ~~Severe Haze Episodes in Beijing, *Journal of Geophysical Research: Atmospheres*, 124, 10248-10263,~~

762 ~~10.1029/2019JD030832, 2019.~~

763 Zhou, W., Xu, W., Kim, H., Zhang, Q., Fu, P., Worsnop, D. R., and Sun, Y.: A review of aerosol chemistry in Asia:

764 insights from aerosol mass spectrometer measurements, ~~*Environ Sci Process*~~*Environmental Science: Processes &*

765 *Impacts*, 22, 1616-1653, 10.1039/d0em00212gDOEM00212G, 2020.

766